Effects of friction and disorder on the quasistatic response of granular solids to a localized force

C. Goldenberg[1,*] and I. Goldhirsch[2,†]

[1]*Laboratoire de Physique et Mécanique des Milieux Hétérogènes (CNRS UMR 7636), ESPCI, 10 rue Vauquelin, 75231 Paris Cedex 05, France*

[2]*School of Mechanical Engineering, Faculty of Engineering, Tel Aviv University, Ramat-Aviv, Tel Aviv 69978, Israel*

(Received 4 November 2007; published 8 April 2008)

The response to a localized force provides a sensitive test for models of stress transmission in granular solids. Elasto-plastic models, traditionally used by engineers, have been challenged by theories and experiments that suggest a wavelike (hyperbolic) propagation of the stress, as opposed to the elliptic equations of static elasticity. Simulations of two-dimensional granular systems subject to a localized external force have been employed to examine the nature of stress transmission in these systems as a function of the magnitude of this force, the frictional parameters, and degree of disorder. The results indicate that in large systems (as considered by engineers) the response is close to that predicted by isotropic elasticity, whereas for small systems (or strongly forced ones) it is strongly anisotropic. In the latter case the applied force induces changes in the contact network accompanied by frictional sliding and gives rise to hyperboliclike stress propagation. The larger the static friction, the more extended the range of forces for which the response is elastic, and the smaller the anisotropy. Increase in the degree of polydispersity (in the studied range, up to 25%) decreases the range of elastic response. This paper is an extension of a previously published Letter [C. Goldenberg and I. Goldhirsch, Nature (London) **435**, 188 (2005)].

DOI: 10.1103/PhysRevE.77.041303 PACS number(s): 83.80.Fg, 45.70.Cc, 81.05.Rm, 46.65.+g

I. INTRODUCTION

Static and quasistatic properties of granular materials are commonly modeled by engineers using elastoplastic [2,3] and hypoplastic [4,5] models. Recently, other types of models have been put forward (mostly by physicists), some of which comprise hyperbolic partial differential equations for the description of stress transmission through these materials [6–11]. The new models, in which stress propagates (much like waves) through the material, are fundamentally different from the (elliptic, elasticlike) old ones, in which the concept of propagating stress does not apply. It seems that this dichotomy started [3,12] in the context of the interpretation of experiments on conical piles [13,14], where a pressure dip below the apex of the pile was observed (the presence of such a dip depends on the construction method [15]).

In order to obtain insights into this problem, it is convenient to consider the simpler geometry of a granular rectangular layer (or slab) resting on a solid support [16], an experimentally well researched system [17–23]. Much as in the case of piles, experiments on granular slabs seem to be sending mixed messages concerning the "correct" description of stress transmission in these systems: some render support to elliptic descriptions whereas others are compatible with hyperbolic models. When the response to the application of an external force is linear in the force (which is the case for sufficiently small forces), the problem is tantamount to the study of the Green's function of the system [22].

The present paper reports results of a detailed study of the response of two-dimensional vertical slabs comprising polydisperse frictional disks subject to gravity and a localized, compressive external load applied at the top of the slab. It significantly expands upon Ref. [1].

The dependence of the response on the magnitude of the external force as well as the interaction parameters and degree of disorder (or polydispersity) has been studied. Our results suggest a resolution of the above-mentioned controversy as well as the seemingly mutually incompatible experimental results. First note that a small localized external force applied to a ("prestressed") static granular system gives rise to excess contact forces and other changes. If the force is sufficiently small, the excess stress can be well described by elasticity and for an isotropic reference configuration by isotropic elasticity (see also [24]). In contrast, a finite external load can cause irreversible rearrangements (loss of contacts, sliding) and strong anisotropy in an *influence zone* in the vicinity of its point of application. Far from this point the excess stress can still be described by elasticity, and therefore sufficiently large systems (for which this zone is basically a point) are expected to exhibit elastic response. Unlike in large systems, the influence zone in a relatively small system can span the entire size of the system and therefore its response will not be elastic but rather hyperboliclike due to the strong anisotropy induced in the zone [3,25]. Frictional forces tend to prevent sliding and loss of contacts; their effect is to shrink the size of the influence zone thus promoting elastic response. As shown below, they also promote isotropy of the response. Therefore, in experiments in which large forces were applied to relatively small systems [17,18,21–23], the observed response could be accounted for by hyperboliclike equations, whereas in other experiments the force was sufficiently small (or the system size sufficiently large) to render the response compatible with elasticity; see, e.g., [18,20,22]. These considerations apply to both ordered (lattice) and disordered (polydisperse) configurations, the main difference being in the ranges of the magnitudes of the external forces for which one observes elastic

*chayg@pmmh.espci.fr

†isaac@eng.tau.ac.il

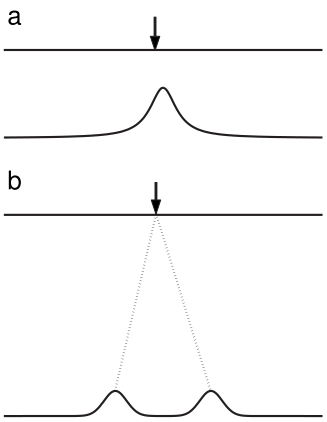

FIG. 1. Predictions of different models, (a) "elliptic" and (b) "hyperbolic," for the response of a granular slab to a localized vertical force applied to its top: excess vertical stress on the floor supporting the slab.

response. Qualitatively similar results were also obtained in a numerical study of the *displacement* response [26]; this study focused on the effect of the mean coordination number, controlled by the particle stiffness. The force network ensemble approach [27] yields qualitatively similar results concerning the effect of friction.

The paper is organized as follows. Section II presents an outline of the elliptic and hyperbolic descriptions of static granular matter and a comparison between the two, as well as results of several relevant experiments. Section III provides a description of the simulation method. Section IV reports the results obtained for frictionless systems, and the subsequent sections describe simulations of more realistic systems, incorporating friction (Sec. V) and disorder or polydispersity (Sec. VI). The results of the simulations and their analysis enable the interpretation of the findings in different experiments; this comprises the content of Sec. VII. Section VIII offers a brief summary and further interpretations.

II. ELLIPTIC VS HYPERBOLIC DESCRIPTIONS

A. Theoretical approaches

As mentioned, the "elliptic" and "hyperbolic" descriptions of stress transmission in granular matter differ both qualitatively and quantitatively. Consider the response on the floor on which a vertical granular slab resides (i.e., the vertical stress at the floor in the presence of an external force minus its value in the absence of this force). Figure 1 illustrates the response to a vertical force applied at the center top of the slab. When isotropic elasticity [28] holds, the response has a single peak, whose width is proportional to the height of the slab, and whose shape is determined by the equations of elasticity and boundary conditions [3,20,29]. In contrast, in hyperbolic models [6–11], the stress propagates along characteristic lines and the response is concentrated on two points in two dimensions (2D) [a ring in three dimensions (3D)]; diffusive broadening broadens the latter into peaks whose width is proportional to the square root of the slab's height [30]. This type of description applies [7–11] to frictionless isostatic systems [31–33], i.e., systems in which the number of equations stemming from Newton's first and third laws equals the number of unknowns (force components), thereby determining the forces. Isostatic systems are marginally stable, and can be considered to comprise plastic materials which are everywhere at incipient yield (and are described by hyperbolic equations [3]). Models based on stress transmission by propagating force chains which may split and merge [34–37] were shown to produce elasticlike equations (in fields whose significance is yet unclear) at large scales [34–36].

A simple 2D model [29] demonstrates that strongly anisotropic elasticity can mimic hyperbolic behavior. The model comprises a triangular lattice of harmonic springs in which the horizontal spring constant K_1 is different from that of an oblique spring, K_2. In the continuum limit this model is described by anisotropic elasticity [for the response of an anisotropic elastic infinite half plane (2D) see [36]]. The nature of the response depends on the degree of anisotropy: it is single peaked for values of K_2/K_1 near 1 ($K_2/K_1=1$ corresponds to an isotropic system), narrower than in the isotropic case for $K_2/K_1<1$, and wider for $K_2/K_1>1$. For sufficiently large values of K_2/K_1, the response is double peaked, as for hyperbolic models. However, the equations of anisotropic elasticity are elliptic, except in the extreme anisotropic limit $K_2/K_1\to\infty$, when they are hyperbolic. This is consistent with the fact that the limit $K_1\to 0$ corresponds to the absence of horizontal springs, which renders the system *isostatic*, much like the well-known example of a square (or cubic) lattice of springs, which (to linear order in the displacements) lacks shear rigidity [38]. Although this anisotropic model is quite artificial, we show below that anisotropy arises naturally in more realistic descriptions of granular materials.

B. Review of experimental results

In the experiments of [18,22], a localized vertical force was applied to a 2D packing of photoelastic particles. The applied forces had to be sufficiently large (about 150 times the particle weight) in order to observe the birefringent patterns [39], based on which the magnitudes of the interparticle forces were estimated [18,22,39]. Three different types of packing, of increasing disorder, were studied in [18,22]: a triangular lattice of nominally monodisperse disks, a packing of bidisperse disks (two different sizes), and a packing of pentagonal particles. Data from 50 configurations were averaged [18,22] for each type of packing. The force profiles as a function of the horizontal (orthogonal to gravity) coordinate (for different depths in each of the slabs) exhibited strong dependence on the degree of disorder: the ordered (lattice) configuration exhibited two prominent "force chains" along the lattice directions (60° to the horizontal), a result which appears to be consistent with a hyperbolic model (however, a vertical force chain, not anticipated by these models, was observed as well). The force chains "faded out" with increasing disorder; for the pentagonal particles the measured force profile possessed a single peak, the width of which varied linearly with the depth, as predicted by elasticity; this led to the suggestion that granular materials experienced a cross-

over from a hyperbolic to an elliptic behavior with increasing disorder [18].

The response of a small 2D slab comprising round-edged rectangular particles [17] exhibits a near-parabolic envelope, as predicted by models that assume an uncorrelated, diffusive propagation of the forces, such as the q model [40,41]. It appears that the envelope may be narrowing down near the bottom of the slab.

The simulations of [23] considered the *displacements* of (rather than force on) disks (of three different diameters) in a 2D packing, induced by a small displacement of a particle at the bottom of the packing. The displacement response is expected to be qualitatively similar to the force response (in isostatic systems the two are equivalent [31,32]). The response profile (averaged over several hundred configurations) possessed a single peak, the width of which appeared to grow as the square root of the system height for small heights, and cross over to a linear dependence for larger heights (these heights were quite small: about ten diameters). The response function (scaled by the width) could be well fitted by a Gaussian. Simulations of isostatic systems presented in the same paper revealed a double-peaked response, as expected.

References [19,20] report the results of experimental measurements of the response at the floor of 3D disordered slabs of sand (and other materials), subject to a weak external localized force (of a few particle weights) at the top of the slab. In this case the response was verified to be linear in the applied force. The response profile was single peaked, its width proportional to the slab height, as expected for an elastic system. The shape of the response was found to depend on the preparation method: it was wider for loose packings (obtained by pulling a sieve through the packing) than for dense packings (obtained by filling the container layer by layer, pressing the packing after each layer is deposited). Isotropic elastic solutions for finite slabs [20] did not fit the results well.

Unlike the disordered systems used in [18,22], the experiments of [21] involved ordered 3D systems of spherical particles, arranged on face-centered cubic (fcc) and hexagonal close-packed (hcp) lattices. The forces on the floor were measured using pressure marks on carbon paper [21]. The applied force was large (a few thousand times the particle weight) for technical reasons. The results were averaged over several packings of nominally equal spheres. For shallow systems, three distinct peaks were observed in the case of the fcc lattice, and a ring for the hcp lattice. This is consistent with a description based on propagating forces [21]. For larger systems the peaks were considerably less distinct, the response being "smoother." This further indicates that a hyperboliclike response may apply only to relatively small systems. For disordered packings [21], a single peak was obtained.

In summary, qualitatively different types of response were observed in experiments on granular assemblies, some of which seem to render support to elliptic models of stress transmission, others to hyperbolic or parabolic models. The degree of disorder plays an important role, as do the size of the system and the magnitude of the applied force. Clearly, other parameters, e.g., the coefficient of friction, may be important as well.

III. SIMULATION METHOD

In order to study the response of granular packings and its dependence on the particle properties, we employ the discrete element simulation method [42,43] (DEM), also known as molecular dynamics (MD) [44–47], to study 2D systems composed of disks. This method has been employed in studies of molecular assemblies as well as granular systems; see, e.g., [48–50] for recent reviews.

A. Force model

Models for grain interactions are usually based on contact mechanics [51,52]. Following Hertz (see, e.g., [28]) and others, one assumes that the forces exerted by solid particles on each other are pairwise additive. Since typical deformations of relatively rigid particles are very small, not-too-soft grains are modeled as being fixed in shape and allowed to slightly overlap; a measure of the overlap is taken to determine the (reversible part of the) normal forces. The tangential forces are taken to depend on the tangential relative particle displacements.

Most natural or industrial granular materials are comprised of nonspherical particles. These are difficult to treat theoretically and even numerically; see, though, the simulations of [53–58]. Therefore we specialize below to homogeneous disk-shaped particles. The force model we use is similar to that employed in [42] (see, e.g., [59–61] for other commonly used force schemes).

The overlap of two spherical or disk-shaped particles is defined by: $\xi_{ij} \equiv R_i + R_j - |\mathbf{r}_{ij}|$, where R_i, R_j are their radii, $\mathbf{r}_i$ is the position of the center (of mass) of particle i, and $\mathbf{r}_{ij} \equiv \mathbf{r}_i - \mathbf{r}_j$. The particles are assumed to interact only when they overlap, i.e., $\xi_{ij} > 0$. Following the classical Hertz theory [28], the force two frictionless elastic spherical particles in contact exert on each other is proportional to $\xi_{ij}^{3/2}$, while for cylinders, it is linear in ξ_{ij} (up to a logarithmic correction [62,63]). In our simulations the normal component (parallel to $\mathbf{r}_{ij}$) of the force is taken to be linear in the overlap (linear springs) so as to simplify the interaction law (further justification is provided by the fact that we consider small deformations, for which one may linearize the force-displacement law around a reference configuration [64]). In addition, a linear (dashpot) viscoelastic damping force [63,65] is employed to model the normal dissipative forces between interacting grains. While hysteretic rate-independent dissipation models (see, e.g., [61,66,67]) may be more realistic, we choose to employ a simple model, since our focus is on static response and small deformations. Therefore the results should not be sensitive to the choice of a dissipation mechanism. All in all, the normal component of the force exerted by particle j on particle i, $\mathbf{f}_{ij}^N$, is modeled by

$$\mathbf{f}_{ij}^N = (k_N \xi_{ij} + \nu_N v_{ij}^N) H(\xi_{ij}) \hat{\mathbf{r}}_{ij}, \tag{1}$$

where $\hat{\mathbf{r}}_{ij} \equiv \frac{\mathbf{r}_{ij}}{\|\mathbf{r}_{ij}\|}$, $v_{ij}^N \equiv (\mathbf{v}_i - \mathbf{v}_j) \cdot \hat{\mathbf{r}}_{ij} \equiv \mathbf{v}_{ij} \cdot \hat{\mathbf{r}}_{ij}$, k_N is the normal spring constant, ν_N is a damping constant, and $H(x)$ is the Heaviside function (equaling 1 for $x > 0$, and 0 for $x < 0$).

Static friction is often modeled [42] by tangential springs which are generated at zero (also rest) length when two par-

ticles establish contact and "snap" when the resulting frictional force f^T satisfies $f^T > \mu_S f^N$, where μ_S denotes the coefficient of static friction, i.e., when the Coulomb limit is exceeded. Once a tangential spring is severed, the corresponding particles can slip with respect to each other and experience dynamic friction, $f^T = \mu_D f^N$, where μ_D denotes the coefficient of dynamic friction, unless the particles separate, in which case they do not interact at all. A velocity-dependent damping term is often used to facilitate relaxation to a static configuration. This description of static friction is consistent with both contact mechanics [51,52] and microscopic theories of friction (see, e.g., [68] for references on friction). The tangential springs are taken to be quite stiff, giving rise to very small, but measurable [69], displacements prior to slip. Tangential springs have often been used to model interparticle interactions in mean-field derivations of granular elasticity [70–73]. More realistic descriptions of frictional contacts account for the history of particle deformations (see, e.g., [59–61,66]).

We model the tangential forces by a spring-dashpot model in conjunction with Coulomb's law of friction, as in [42]. The coefficients of static and dynamic friction are taken to equal each other: $\mu_D = \mu_S = \mu$ (since this work focuses on static configurations, the precise value of μ_D is not of importance, as it only affects the evolution toward these configurations). The tangential component of the relative velocity at a contact (in 2D) is given by

$$\mathbf{v}_{ij}^T = \mathbf{v}_{ij} - v_{ij}^N \hat{\mathbf{r}}_{ij} - \hat{\mathbf{t}}_{ij}(R_i\omega_i + R_j\omega_j), \tag{2}$$

where $\omega_i \equiv \dot{\theta}_i$ is the angular velocity of particle i, θ_i denotes the particle's rotation angle, and $\hat{\mathbf{t}}_{ij} \equiv \hat{\mathbf{z}} \times \hat{\mathbf{r}}_{ij}$. Thus, the model we use for the tangential forces is

$$\mathbf{f}_{ij}^T = (-k_T \mathbf{s}_{ij} - \nu_T \mathbf{v}_{ij}^T) H(\xi_{ij}), \tag{3}$$

where k_T is the tangential spring constant and the spring length $\mathbf{s}_{ij}$ obeys

$$\dot{\mathbf{s}}_{ij} = [\mathbf{v}_{ij}^T + (\dot{\mathbf{s}}_{ij} \cdot \hat{\mathbf{t}}_{ij})\hat{\mathbf{t}}_{ij}] H(|\mu \mathbf{f}_{ij}^N| - k_T |\mathbf{s}_{ij}|), \tag{4}$$

which ensures that the spring is always tangent to the plane of contact (a line in 2D), and does not exceed the length that corresponds to the Coulomb limit. In addition, $\mathbf{s}_{ij}$ is set to zero if there is no overlap (i.e., $\xi_{ij} < 0$). The tangential displacement is obtained by integrating Eq. (4) from the time the particles establish contact. When $\mathbf{f}_{ij}^T$ becomes equal to $\mu \mathbf{f}_{ij}^N$, the length of the tangential spring is kept fixed in order to prevent the frictional force from exceeding the Coulomb limit. This is important in order to avoid unrealistic behavior when the contacts cease sliding (i.e., $f^T = \mu f^N$), and revert to sticking ($f^T < \mu f^N$) [74]: if the integration of the tangential velocity were to be continued for a sliding contact, and the result used to further stretch the tangential spring, an unrealistically large force would be obtained when the contact reverts to sticking. Note that the torques exerted on the particles determine their angular accelerations; the corresponding equations are part of the system of equations that are solved.

The interactions of the particles with the walls are similar to the interparticle interactions. Since the walls considered here are rigid (fixed) straight lines (in 2D), the overlaps are calculated accordingly, with the same force models. The force constants for particle-wall interactions, $(k_N^{\text{wall}}, k_T^{\text{wall}}, \nu_N^{\text{wall}}, \nu_T^{\text{wall}}, \mu^{\text{wall}})$, may be specified to be different from those used for particle-particle interactions (which are taken to be the same for all particle pairs). In addition to interparticle and particle-wall forces, gravity is accounted for as well. External forces and torques may also be applied to specific particles (see below).

B. Parameters

The studied systems comprise collections of polydisperse disks, whose radii are uniformly distributed in the interval $[R - \delta R, R]$. In order to facilitate the use of parameters from experiments performed on short cylinders, the cylinder thickness W and its mass density ρ are specified, and the particle masses are given by $m_i = \pi R_i^2 W \rho$. We consider the case of homogeneous disks, for which the axial moment of inertia is given by $I_i = \frac{1}{2} m_i R_i^2$. The parameters used in this work correspond to experiments performed by Geng and Behringer using 2D photoelastic disks [75]: $R = 3.75 \times 10^{-3}$ m, $W = 6.6 \times 10^{-3}$ m, and $\rho = 1.15 \times 10^3$ kg/m^3.

The simulation results are presented in terms of nondimensional quantities: the length unit is the mean particle radius $\bar{R}$, the time unit is $\tau = \sqrt{\bar{R}/g}$ (where g is the magnitude of the acceleration of gravity; its value in the simulations is set to 9.8 m/s^2), and the mass unit is the mean particle mass $\bar{m}$.

The value of the spring constant k_N for the normal springs is taken to equal $3000\bar{m}g/\bar{R}$. This value is based on force-displacement measurements performed on the photoelastic disks used in [64]. Although the particles are cylindrical, measurements showed a force proportional to the $\frac{3}{2}$ power of the displacement (possibly indicating an elliptic, rather than rectangular, area of contact). However, for the typical deformations obtained in the experiments, a linear fit to the particle force law provides quite a good description [64], further justifying our choice of linear springs. For the particle-wall interactions, we use $k_N^{\text{wall}} = 2k_N$.

The damping coefficient is chosen to equal half its critical value for an individual contact, $\nu_c = 2\sqrt{k}$ (recall that k and ν are nondimensional), i.e., we use $\nu_{N,T} = \sqrt{k_{N,T}}$. This value was found to produce the fastest relaxation of the system toward static equilibrium and is irrelevant in the state of mechanical equilibrium itself.

Other simulation parameters such as the ratio k_T/k_N (and $k_T^{\text{wall}}/k_N^{\text{wall}}$, taken to equal it), the coefficients of friction μ and μ^{wall}, and the degree of polydispersity δ were varied in different runs.

C. Simulation procedure and initial conditions

The equations of motion were integrated using the Beeman algorithm [45], which provides more accurate velocities than the commonly used Verlet algorithm [45]. The use of a Gear five-value predictor-corrector algorithm [47] did not yield any significant changes in the results. We used $\Delta t = 5$

$\times 10^{-4}\tau = 5 \times 10^{-4}\sqrt{\bar{R}/g}$ as the time step; decreasing it below this value did not affect the results.

The initial configuration was produced by placing the particles on a triangular lattice of lattice constant $2\bar{R}$. The sidewalls and the floor were placed at a distance $\bar{R}$ from the centers of the particles closest to them (so that for a monodisperse packing these particles were tangent to the sidewalls and the floor). The initial (translational and angular) velocities of all particles were set to zero. The next step was to allow the system to relax under gravity until static equilibrium was reached, as further described below. The typical time needed to obtain proper relaxation (see below) was between τ and 30τ.

In order to study the response to a localized force, the resulting configuration (with all velocities reset to zero) was used as an initial configuration for a second run of the simulation, in which an external force (and/or torque in some simulations) was applied to a particle at the center of the top row of particles. The force was linearly increased, during a time τ, from zero to its desired value. The system was then relaxed again to static equilibrium.

The criterion for static equilibrium was that the kinetic energy per particle was sufficiently small. We found that, in order to obtain an error of less than 1% for the forces exerted on the floor in practically any realization, the system had to be relaxed to a kinetic energy of $E_k^{\mathrm{stop}} = 10^{-13}\bar{m}g\bar{R}$ per particle, which is significantly smaller than that used in previous studies (e.g., in [76], the systems were relaxed to $E_k^{\mathrm{stop}} = 2 \times 10^{-8}\bar{m}g\bar{R}$ per particle). For polydisperse systems the response was coarse grained and averaged over a number of different configurations (Sec. VI), since it exhibited strong fluctuations. In this case, sufficient accuracy was obtained with $E_k^{\mathrm{stop}} = 10^{-9}\bar{m}g\bar{R}$. We verified that several other criteria for static equilibrium (see [77]) were satisfied: the contact network was fixed for at least several hundred time steps, during which each particle had at least two contacts, there were no sliding contacts, and the mean particle acceleration was less than $10^{-5}g$.

For frictionless systems ($\mu = \mu^{\mathrm{wall}} = 0$), we found that reaching such small energies in a reasonable simulation time was difficult due to the existence of slow global modes with a low dissipation rate. Therefore the following algorithm was used for accelerating the relaxation in this case: the MD simulation was stopped at a higher energy ($E_k^{\mathrm{stop}} = 10^{-6}\bar{m}g\bar{R}$). The configuration obtained at this stage was used as a reference state around which the linearized equations of motion were iteratively solved to approach a static equilibrium. In each iteration the equations were solved by matrix (pseudo)inversion, and the connectivity of the particles was updated to ensure that there was no tension. The iterations were stopped when the maximal relative particle displacement was less than $10^{-14}\bar{R}$ (the numerical accuracy). The typical kinetic energy obtained this way was less than $E_k = 10^{-22}\bar{m}g\bar{R}$ per particle. This configuration was then used for calculating the interparticle forces in the absence of an external force and as an initial condition for the process of application of this force. An example of the interparticle forces obtained in a typical simulation run is presented in Fig. 2. In order to calculate the response, the forces due to gravity alone (without the applied force) were vectorially subtracted at each contact.

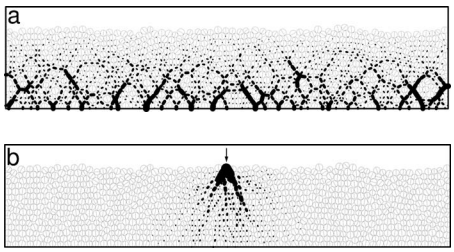

FIG. 2. Forces obtained in a simulation of a polydisperse ($\delta = 0.25$) frictional system composed of 15 layers of 60 particles each, with $k_T/k_N = 0.8$ and $\mu = \mu^{\mathrm{wall}} = 0.2$. The linewidths and lengths are proportional to the force magnitudes. (a) After relaxation under gravity; (b) after relaxation with an additional vertical force $F_{\mathrm{ext}} = 5\bar{m}g$ at $\downarrow$, where $\bar{m}$ is the mean particle mass, with the forces obtained in (a) subtracted. The lines drawn inside the particles indicate the rotation angles: in the initial configuration (before relaxation under gravity) the lines are vertical. The arrow denotes the position of the externally applied force.

IV. RESPONSE OF FRICTIONLESS SLABS

In this section, we describe the results of simulations of systems of monodisperse frictionless particles. The interparticle force in this case is parallel to the normal direction and given by Eq. (1). As shown in [29], the application of a localized force at the top of a frictionless packing can lead to rearrangements in the contact network: horizontal springs in a region below the point of application of the force are severed (as also observed in [78] for a pile geometry). Interestingly, the force chains in this system are qualitatively similar to those obtained [29] when the particle interactions are modeled by regular "two-sided" springs (which do not snap under tension). However, the dependence of the force magnitudes on the horizontal coordinate at different depths is in better agreement with experiment, as expected (see Fig. 4 in [29]), when the particle interactions are modeled by "one-sided" springs [18,22], as described by Eq. (1). The reason is that the latter model is more realistic since it does not allow the establishment of tensile forces [29]. The stress distribution at the floor for unilateral springs [29] may be anisotropic, and exhibit two peaks. As mentioned, this anisotropy is related to the existence of a region of open horizontal contacts where the anisotropy is large and the hyperbolic limit applies [29]. The anisotropy is not present in the absence of the external forces or, as shown below, far from the point of application of an external force or when it is sufficiently small. The dynamical process leading to this anisotropy is of nonlinear nature as it involves changes in the contact network induced by the externally applied forces [29]. It may be possible to model the corresponding dynamics by a nonlinear extension of linear elastic theory in which the elastic moduli are stress history dependent (in particular, the anisotropy induced by the opening of contacts in certain regions may be considered to result from an attempted ten-

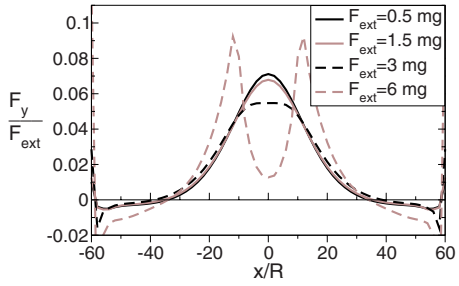

FIG. 3. (Color online) Response of frictionless ordered systems for different applied forces F_{ext}.

sile stress in these regions). Stress-induced anisotropy has also been discussed in the context of plastic models of soil mechanics [79] as well as nonlinear elastic models [24]. If the particle positions do not change appreciably so that only the contact network is modified in response to the applied force (or stress), the behavior can possibly be modeled as "incrementally elastic." Under certain conditions (corresponding to plastic yield) the system is no longer able to support the applied stress without a major rearrangement of the particles. Incipient plastic yield may be related to a local extreme anisotropy typical of a marginally stable, locally isostatic, configuration.

A. Dependence on the applied force: Crossover from hyperboliclike to elliptic response

In order to examine the changes in the contact network in more detail, we performed DEM simulations, as described in Sec. III, of a system similar to those discussed in [29], with different applied forces. We focused on systems of 15 layers of 60 particles each; the effect of the system size is discussed below. The force response on the floor is shown in Fig. 3. A crossover from a single- to a double-peaked response occurs as the applied force is increased. The changes in the contact network corresponding to the systems of Fig. 3 are shown in Fig. 4. For a sufficiently small force (not shown), the contact network is unchanged, and the response is fully elastic (see Sec. V for a discussion of the linearity of the response). As the force is increased, horizontal contacts are opened in a teardrop-shaped region below the point of application of the force, whose size increases with the force (and in the frictional case decreases with friction; see below). As mentioned, in this region the extreme anisotropic limit of elasticity applies. When the teardrop is sufficiently far from the floor [Figs. 4(a) and 4(b)], the response at the floor is single peaked, as the changes induced by the force are basically localized. Otherwise, the anisotropy induced by the external force reaches the floor [Fig. 4(c)], inducing a double-peaked response (the crossover actually occurs at slightly smaller forces, at which the teardrop almost reaches the floor).

B. Dependence on system size

The dependence of the crossover on the size of the system is important for the interpretation of experimental results. The depth and maximal width of the teardrop as a function of

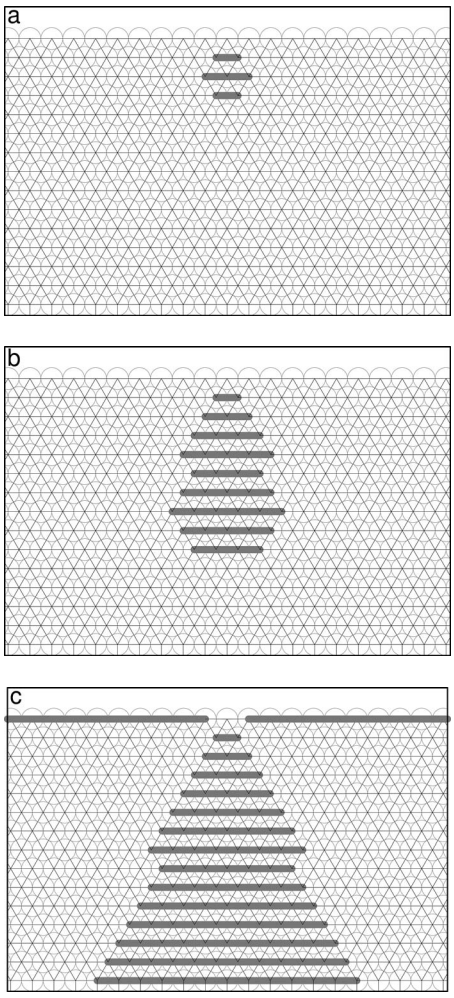

FIG. 4. Changes in the contact network in an ordered frictionless system for different applied forces: F_{ext}= (a) 1.5 mg, (b) 3 mg, and (c) 6 mg. The central third of the system is shown. Thick lines connecting particle centers indicate contacts opened due to the application of the force; thin lines represent contacts that are unaffected.

the applied force, for several system sizes, are plotted in Fig. 5. It is seen that the size of the teardrop slightly decreases as the height of the slab increases. This indicates that the changes in the contact network induced by the external force can be considered to be finite-size effects [1], whose importance decreases as the size of the system increases. For identical external loads, very deep systems (as typically found in nature and in engineering applications) are expected to exhibit a single-peaked response, whereas relatively shallow ones, as studied in some experiments (Sec. II B), should exhibit two peaks. This is one of the reasons that different experiments, using differently sized samples, yield qualitatively different results. This observation also applies when frictional interactions are accounted for, as described in Sec. V.

C. Dependence on particle stiffness

The effect of the particle stiffness is considered next. Simulations with different values of k_N reveal that the size of

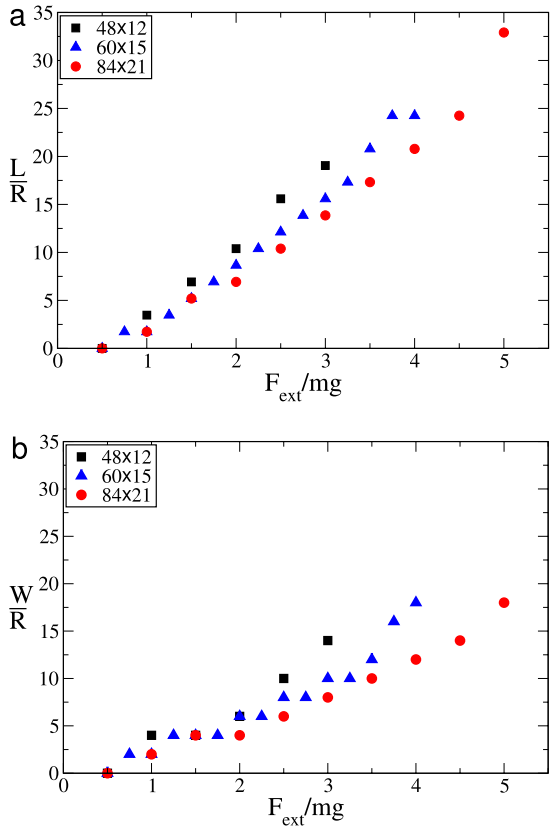

FIG. 5. (Color online) (a) Depth L and (b) maximal width W of the teardrop in units of the particle radius R in ordered (monodisperse) frictionless systems (Fig. 4), as a function of the applied force, normalized by the weight of a particle, for different system sizes.

the teardrop increases with the stiffness of the particles but appears to saturate for $k_N \gtrsim 2000\ \mathrm{mg}/R$. The results presented here pertain to $k_N = 3000\ \mathrm{mg}/R$. In practical terms, the response is quite insensitive to the choice of stiffness for $k_N \gtrsim 1000\ \mathrm{mg}/R$, e.g., at $x=0$, it only changes by about 2% in the range $1000\ \mathrm{mg}/R < k_N < 10^5\ \mathrm{mg}/R$. It follows that the crossover from a single- to a double-peaked response is essentially independent of the particle rigidity, provided that the particles are sufficiently stiff; otherwise the particle overlaps may be appreciable and the external force may lead to significant rearrangements.

The lack of dependence of the response on the particle stiffness may be understood as follows. In the reference configuration, contacts are compressed due to gravity as well as the effects of the rigid immobile walls and floor (the application of an external pressure to the system can result in a similar effect). In contrast, the application of the external force leads to attempted tensile interparticle forces which may overpower the compressive forces present in the system. Therefore the opening of contacts is determined directly by the local stress, rather than the local strain (which does depend on the particle stiffness) when the geometry of the system is not significantly affected by the applied force. This justifies our choice of the particle weight as the unit of force (rather than a scale based on the particle stiffness and size).

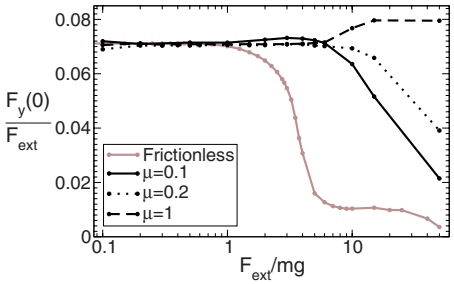

FIG. 6. (Color online) Response at $x=0$ of ordered systems, normalized by the applied force F_{ext}, vs the applied force (in units of the particle weight mg), for different coefficients of friction μ, frictionless walls ($\mu^{\mathrm{wall}}=0$), and $k_T/k_N=0.8$.

The same behavior may persist even as $k_N \to \infty$ under the same boundary conditions, provided that the particles in the reference state are still in contact along the horizontal direction. However, as the stiffness increases, this requirement may be hard to comply with, as the particles must fit exactly between the walls in order to remain in contact: in the limit $k_N \to \infty$ most horizontal contacts may be absent already in the reference state, rendering it isostatic, and this would lead to a hyperboliclike response even for an infinitesimal applied force, as suggested in, e.g., [7–11]. Therefore the above "limit of infinite stiffness" should be understood as "large but finite" stiffness (the physically relevant case) else isostaticity comes into play. Furthermore, one must bear in mind that frictionless particles are a rather artificial idealization in the context of granular materials. Indeed, as shown in the next section, the presence of friction affects the behavior of the system is a significant way and, in particular, renders it less sensitive to the contact network.

V. EFFECTS OF FRICTION

A. Dependence on the applied force: Friction increases the linear range

As mentioned in Sec. IV, sufficiently small external forces do not induce changes in the contact network, so that the response is expected to be linear in the applied force [80]. This is demonstrated in Fig. 6, which presents the response on the floor at $x=0$ (below the point of application of the force) as a function of the applied force, in both frictionless and frictional systems (with $k_T/k_N=0.8$; the effect of this parameter is discussed below). The results shown were obtained with frictionless walls ($\mu^{\mathrm{wall}}=0$; see Sec. III), since for weak applied forces, frictional walls can support some of the load, inducing nonlinearity in the response. A linear (*elastic*) range is observed for sufficiently small applied forces even for frictionless particles, due to the fact that the particles are slightly deformed by gravity, and a small force does not cause the contacts to open.

Figure 6 shows that friction has a significant effect on the linearity of the response: The extent of the linear range is significantly larger (by almost an order of magnitude) in frictional systems; thus elasticity is enhanced by friction.

The effect of friction on the response profile is shown in Fig. 7 for different applied forces, for $\mu=0.2$ and 1 (compare

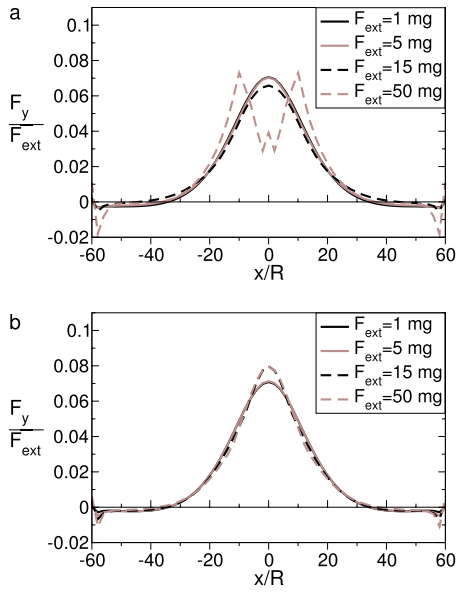

FIG. 7. (Color online) Response of ordered systems, with different coefficients of friction $\mu=$ (a) 0.2 and (b) 1, to applied forces (F_{ext}) of different magnitudes, frictionless walls ($\mu^{\text{wall}}=0$), and $k_T/k_N=0.8$ (compare to Fig. 3).

to the frictionless case presented in Fig. 3). Note that the force for which the crossover from a single- to a double-peaked response occurs increases rapidly with friction (as also observed in Fig. 6), so that friction renders the response closer to that expected from *isotropic* elasticity. For $\mu=1$ no crossover is observed even for the largest force shown, $F_{\text{ext}}=50$ mg (a different type of crossover occurs for $\mu=1$ for larger forces; see Sec. V E). Sufficiently large forces may induce major rearrangements (i.e., plastic flow), not considered here.

B. Effect of friction on the contact network

To gain a better understanding of the effect of friction on the response, we examine the changes in the contact network. Our simulations reveal that the first contact is opened when $F_{\text{ext}}=0.75$ mg in the frictionless case, $F_{\text{ext}}=4$ mg for $\mu=0.2$, and $F_{\text{ext}}=6$ mg for $\mu=1$. This is compatible with the fact that the range of forces for which the response is linear is larger in frictional systems than in frictionless ones.

The effect of the applied force on the changes in the contact network in a system with $\mu=0.2$ is shown in Fig. 8 (compare to Fig. 4). For the same force, the region of open horizontal contacts is considerably smaller in the frictional case than in the frictionless case [compare Figs. 4(c) and 8(a)]. In addition, in the frictional case this region reaches the floor for a much larger force [compare Figs. 4(c) and 8(c)]. This is why the crossover to a double-peaked response, associated with the anisotropy in this region, occurs at larger forces in the frictional case.

The above mechanism does not explain the findings for $\mu=1$ (or larger coefficients of friction, in general), for which the response is single peaked even for rather large forces [see Fig. 7(b)], for which the region of open contacts (Fig. 9)

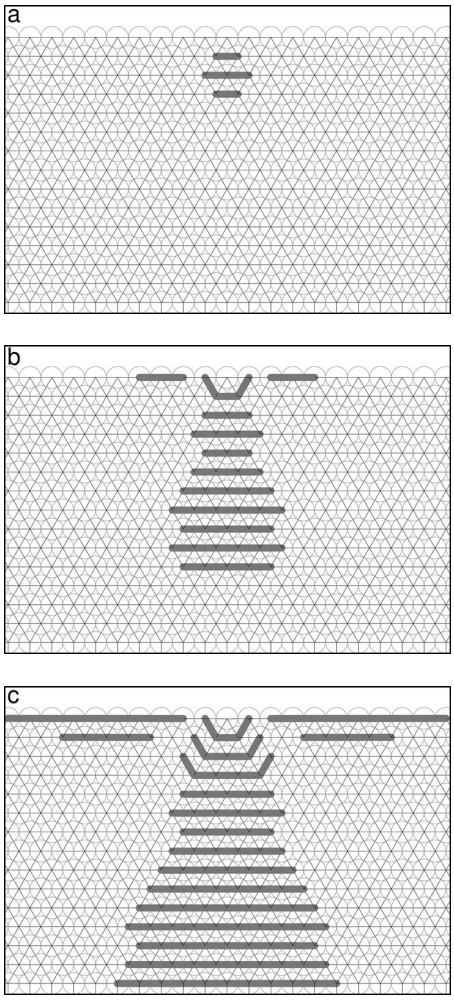

FIG. 8. Changes in the contact network in a frictional system with $\mu=0.2$, with different applied forces $F_{\text{ext}}=$ (a) 6 mg, (b) 15 mg, and (c) 50 mg, frictionless walls ($\mu^{\text{wall}}=0$), and $k_T/k_N=0.8$. The various lines are explained in the caption of Fig. 4.

reaches the floor (it does so even for a smaller force than in the case of $\mu=0.2$). In addition, the profile of the response in this case is narrower than for small coefficients of friction (see, however, Sec. V E), These results suggest that the degree to which the external force changes the contact network is not the only factor affecting the response. As mentioned above, a hyperboliclike response is the result of anisotropy, irrespective of its origin. Changes in the contact network can indeed induce anisotropy but, as it turns out, friction can partially restore isotropy in regions with abundance of open contacts by introducing forces in additional directions (see more below). Note that, when μ is sufficiently large (and F_{ext} sufficiently small), its value is essentially immaterial, since sliding is practically precluded. In this case, the ratio of the tangential to normal stiffness, k_T/k_N (see Sec. III A), determines the response. Figure 10 presents the response obtained for different values of k_T/k_N, $F_{\text{ext}}=15$ mg, and $\mu=10$ (which is practically equivalent to $\mu=\infty$, as used in [26], since no sliding occurs). A crossover from a single- to a double-peaked response occurs with *decreasing* k_T/k_N (the crossover occurs at $k_T/k_N\simeq 0.3$). For larger values of k_T/k_N, the re-

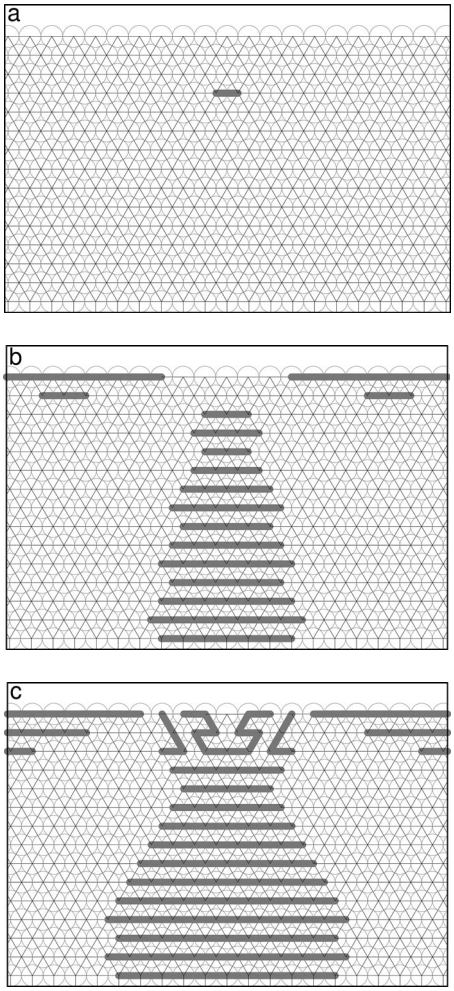

FIG. 9. Changes in the contact network in a frictional system with $\mu=1$, with different applied forces $F_{\text{ext}}=$ (a) 6 mg, (b) 15 mg, and (c) 50 mg, frictionless walls ($\mu^{\text{wall}}=0$), and $k_T/k_N=0.8$.

sponse is nearly independent of k_T/k_N. This phenomenon is further studied immediately below.

C. Large friction: The role of tangential stiffness

In order to understand the dependence of the response on k_T/k_N, we consider a 2D spring network similar to that described in [29] (i.e., a triangular lattice with different spring constants for horizontal, k_1^n, and oblique, k_2^n, springs). In addition, this model (see Fig. 11) includes tangential springs (as used in our DEM simulations; Sec. III A), whose constants are different for horizontal, k_1^t, and oblique, k_2^t, contacts [80]. Note that for Hertzian interactions the existence of anisotropic prestress (e.g., due to gravity) may indeed result in different spring constants in the horizontal and oblique directions. This model does not incorporate sliding, so that it corresponds to $\mu=\infty$. Similar models were studied in [70,81,82], and more recently in [36,73,83], where equal spring constants were used in all lattice directions.

The elastic moduli corresponding to the long-wavelength limit of this model can be calculated as follows. To leading

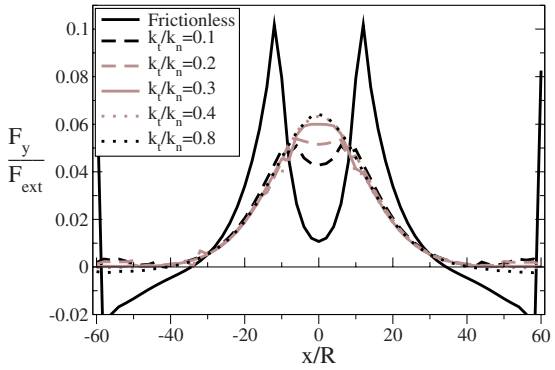

FIG. 10. (Color online) Response of ordered systems for a large coefficient of friction ($\mu=10$) and different values of the ratio of tangential to normal stiffness, k_T/k_N, with $F_{\text{ext}}=15$ mg.

order in the relative particle displacements $\mathbf{u}_{ij}$ (which is the relevant order for linear elasticity), the elastic energy of the system is given by

$$E^{\text{el}} = \frac{1}{2}\sum_{\langle ij\rangle} k_{ij}^n(\hat{r}_{ij}\cdot\mathbf{u}_{ij})^2 + k_{ij}^t[\mathbf{u}_{ij} - (\hat{r}_{ij}\cdot\mathbf{u}_{ij})\hat{r}_{ij}]^2, \qquad (5)$$

where the sum is over nearest neighbors; see Fig. 11 for the assignment of spring constants. A homogeneous affine deformation is defined by a symmetric, uniform strain field: $u_{ij\alpha}(\mathbf{r},t)=\epsilon_{\alpha\beta}r_{ij\beta}$. Note that when tangential forces are present, the stress is not necessarily symmetric (as assumed in classical elasticity); however, the micropolar terms due to this asymmetry are of higher order in the strain. We verified that they were very small, even near the point of application of the external force: there the magnitude of the antisymmetric part of the stress is only a few percent of the pressure.

Using the notation of [36],

$$E^{\text{el}} = \frac{1}{2}\begin{pmatrix}\epsilon_{xx}\\ \epsilon_{zz}\\ \epsilon_{xz}\end{pmatrix}^T\begin{pmatrix}a & c & 0\\ c & b & 0\\ 0 & 0 & d\end{pmatrix}\begin{pmatrix}\epsilon_{xx}\\ \epsilon_{zz}\\ \epsilon_{xz}\end{pmatrix}, \qquad (6)$$

where the superscript T denotes the transpose, one obtains the following elastic moduli:

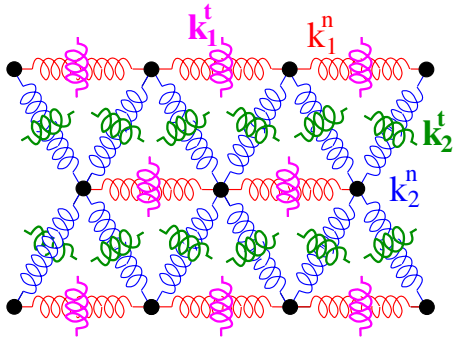

FIG. 11. (Color online) Spring model with normal and tangential springs.

$$a = \frac{R^2}{2A}(8k_1^n + k_2^n + 3k_2^t), \tag{7}$$

$$b = \frac{R^2}{2A}(9k_2^n + 3k_2^t), \tag{8}$$

$$c = \frac{R^2}{2A}(3k_2^n - 3k_2^t), \tag{9}$$

$$d = \frac{R^2}{2A}(6k_2^n + 4k_1^t + 2k_2^t), \tag{10}$$

where $A=2\sqrt{3}R^2$ is the area of the unit cell. These results are consistent with those obtained in [36] for normal springs only, but different from the model with bending interactions introduced in [36].

In a domain of open horizontal contacts one has $k_1^n=k_1^t=0$. It was already shown in Sec. IV that, in the absence of tangential forces ($k_2^t=0$), this system corresponds to the extreme anisotropic limit. However, since the oblique tangential springs apply forces that have horizontal components, they can (at least partially) compensate for the absence of normal horizontal springs, and therefore significantly decrease the anisotropy.

Otto *et al.* [36] presented continuum elastic solutions for an anisotropic infinite half plane subject to a localized force. They found a criterion for the determination of the nature of the response [36]: two peaks are expected for $r \equiv \frac{1}{bd}[ab - c(d+c)] < 0$. Note that this criterion refers to an infinite half plane rather than a slab of finite height, which is more appropriate for describing our simulations. In addition, this model is homogeneous, while the region of open contacts (even when it reaches the floor) is roughly a triangle below the point of application of the force. Nevertheless, the estimate obtained using this criterion fits our result for the finite slab quite well: for the model used here (with no horizontal springs), $r=\frac{\beta^2+10\beta-3}{\beta^2+6\beta+9}$, where $\beta \equiv k_2^t/k_2^n$. Hence (in the physically relevant range $\beta>0$), two peaks are expected for $\beta \lesssim 0.2915$, which is consistent with the value $k_T/k_N \simeq 0.3$ obtained in the simulation (Fig. 10).

For an infinitesimal tangential load applied to a system composed of elastic spheres, the Cattaneo-Mindlin model [52] yields $k_T/k_N=\frac{2(1-\nu)}{2-\nu}$, where ν is the Poisson ratio of the spheres. For the range of positive Poisson ratios ($0 \le \nu \le 0.5$; notice that this is a 3D Poisson ratio), this implies that $2/3 \le k_T/k_N \le 1$, so that the minimal value of k_T/k_N is well above the crossover from two peaks to one. In most of the simulations presented in this work, we use $k_T/k_N=0.8$, which corresponds to a realistic Poisson ratio of about 0.3. We would like to stress that simulations in which the value of k_T/k_N is taken to be too small may produce unphysical results.

D. More on the effects of friction

The above results show that static friction acts to retain an "effective connectivity" among the grains when the horizontal contacts are open, and renders the system more isotropic than one would have naively anticipated. However, since the frictional forces are limited by the Coulomb condition ($f^T \le \mu f^N$; see Sec. III A), sliding can occur if μ is too small (or F_{ext} large). This increases the anisotropy, since not all tangential springs can exert as large forces as predicted by the above model (in which $\mu=\infty$), and leads to a crossover to a double-peaked response. This crossover is shown as a function of μ (for $F_{\text{ext}}=15$ mg) in Fig. 12. Note that, unlike the coefficient of dynamic friction, which is typically smaller than 1, the *effective* coefficient of static friction (which determines the onset of sliding) may be significantly larger than 1 for rough spherical particles, and certainly for irregularly shaped particles (which can interlock and avoid relative rotation).

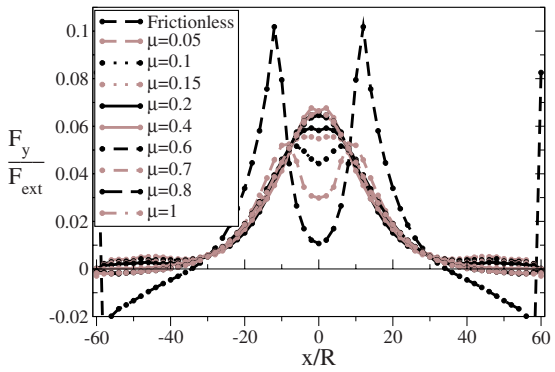

FIG. 12. (Color online) Response of ordered systems for $k_T/k_N=0.8$ and different values of μ with $F_{\text{ext}}=15$ mg.

For $\mu=0.2$, the region of open horizontal contacts (the teardrop) reaches the floor for $F_{\text{ext}} \simeq 20$ mg, which is close to the crossover force [see Fig. 16(a)]. Sliding occurs in the system (mainly near the point of application) even for smaller forces, and the area of sliding contacts gradually spreads downward with increasing F_{ext}. It therefore appears that the crossover for $\mu=0.2$ is associated with the reduction, due to sliding, of the compensating effect of the tangential forces. For sufficiently large forces ($F_{\text{ext}} \gtrsim 40$ mg) the response, for $\mu=0.2$, exhibits a small third peak at $x=0$ [below the point of application of the external force; see Fig. 16(a)]; it is induced by a reorganization of the sliding contacts within the teardrop.

Note the short vertical force chain in Figs. 13(b) and 13(c), which is in conformity with experiment [18,22]. This is yet another important consequence of friction, namely, that the forces (hence the force chains) no longer need to be aligned with the lattice directions, as they are in the absence of tangential forces. In general the inclusion of friction in the models begets a better fit to experiment. In particular our results nicely reproduce the experimental findings obtained in [18,22] for monodisperse packings: the force magnitudes vs the horizontal coordinate at different depths for $\mu=1$ (for the particles used in the experiments, $\mu \simeq 0.94$ [75]) are shown in Fig. 14(b); compare to the frictionless case, Fig. 14(a). We also reproduce [84] force chains along nonlattice directions observed in experiments with applied forces at oblique angles [22], using simulations of frictional particles (with some polydispersity; see Sec. VI below).

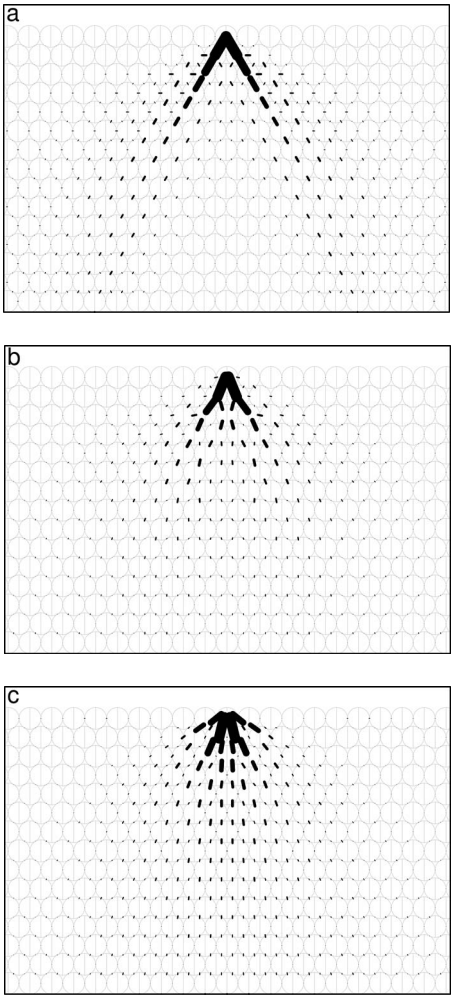

FIG. 13. Interparticle forces in ordered systems with different coefficients of friction $\mu=$ (a) 0, (b) 0.2, and (c) 1 ($\mu^{\text{wall}}=\mu$, $k_T/k_N=0.8$), with $F_{\text{ext}}=15$ mg. The effect of gravity has been subtracted. The central third of the system is shown. Linewidths and lengths are proportional to the force magnitude.

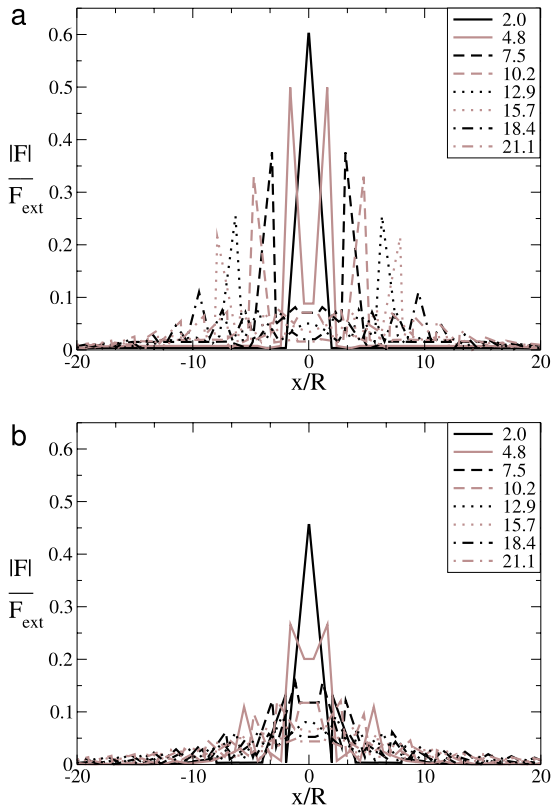

FIG. 14. (Color online) Norms of the interparticle forces, $|\mathbf{f}|$, vs the horizontal position x in ordered systems, for an applied force of magnitude $F_{\text{ext}}=150$ mg. The legend indicates the depth measured from point of application of the force, in particle radii (compare to the experimental measurements shown in [18,22]). (a) Frictionless particles; (b) frictional particles with $\mu^{\text{wall}}=\mu=1$ and $k_T/k_N=0.8$.

It is not surprising that the effects of friction are also evident in the vertical stress component σ_{zz} (Fig. 15), whose calculation is based on [29,85]. In particular, the reduced anisotropy is apparent in the stress field (the stress field for $\mu=1$ is similar to that obtained in the case of an isotropic harmonic lattice [29]).

E. Symmetry breaking for $\mu=1$

For $\mu=1$ we have seen that the response is very different from that obtained for $\mu=0.2$. It remains single peaked (and becomes narrower) for rather large forces, much beyond those for which the crossover is obtained for $\mu=0.2$ [see Fig. 7(b)]. However, when the force exceeds $F_{\text{ext}}=91$ mg, a transition to an *asymmetric* response [see Fig. 16(b)] occurs (unlike the symmetric double-peaked response obtained for lower friction and large forces). The type of asymmetry (favoring positive or negative values of x) appears to be related to the transient vibrations excited by the application of the external force; for some close pairs of forces [e.g., $F_{\text{ext}}=92$ mg and 95 mg; see Fig. 16(b)], the rescaled response to one force is nearly the mirror image (with respect to $x=0$) of the response to the other. The shape of the response remains qualitatively similar for much larger F_{ext}. The transition to an asymmetric response is accompanied by a significant change in the contact network (which becomes asymmetric itself), and leads to a marked *reduction* in the number of sliding contacts.

This instability process, though appears to be dominated by sliding, rather than changes in the contact network. Its source and the particular mechanism of symmetry breaking require further study. It is possible that the instability is related to shear banding. It also bears some similarities to elastic buckling (which is, however, outside the realm of linear elasticity).

F. Pile geometry

While the work reported here focuses on the response of a granular slab, we also examined the effect of friction on a pile composed of 11 layers of monodisperse disks arranged on a triangular lattice, prepared as described in Sec. III C (similar to the frictionless piles in [78]). These piles are quite unrealistic, since the sides of the pile are at 30° to the horizontal, which is larger than the angle of repose for disks.

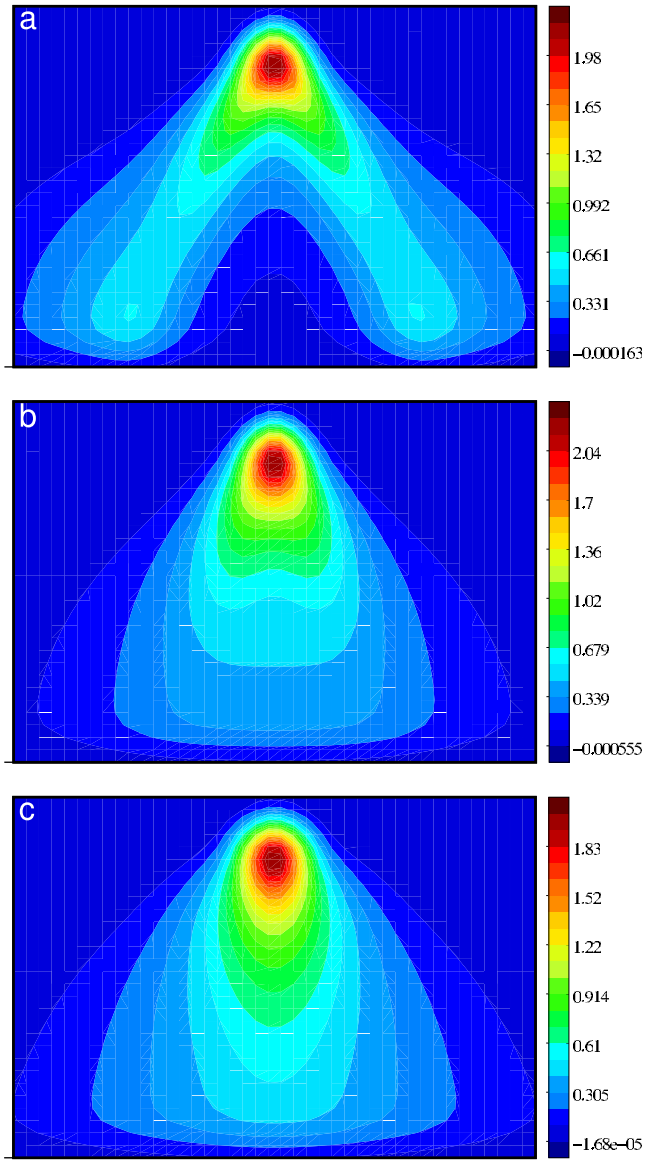

FIG. 15. (Color online) Contour plot of the vertical stress response σ_{zz} in the systems shown in Fig. 13, calculated using a Gaussian coarse-graining function of width $w=2R$.

Therefore, the edges of the pile have to be supported by sidewalls (the construction of stable piles on a smooth floor requires the introduction of *rolling friction*, or rolling resistance [86]).

The forces and the corresponding vertical stress component σ_{zz} in the pile are shown in Figs. 17(a)–17(d). As in the case of the slab (Figs. 13 and 15), the effect of friction is significant. In particular, as shown in Figs. 17(c) and 17(d), the pile of frictionless disks exhibits a dip in the stress under the apex, but that of frictional disks does not. The dip in the frictionless case is due to the open horizontal contacts in the central region of the pile; see Fig. 17(e). In the frictional case, the size of the region of open contacts in the central region of the pile is quite similar, but its shape is different [Fig. 17(f)]. The absence of the dip results from the reduced anisotropy due to the frictional forces, as discussed above for the slab geometry. We therefore conclude that the presence

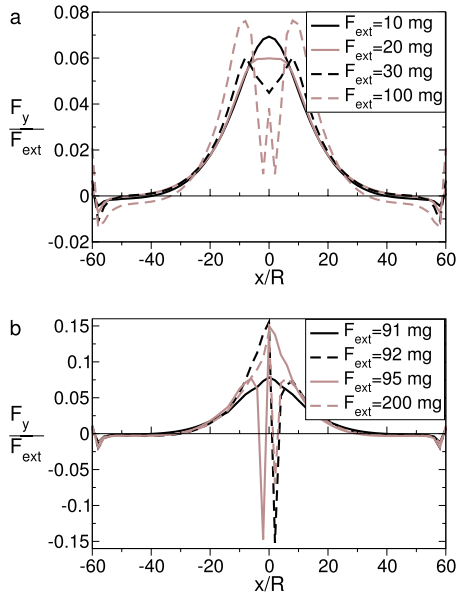

FIG. 16. (Color online) Response of ordered systems, with different coefficients of friction (a) $\mu=$ (a) 0.2 and (b) 1, to different magnitudes of the applied force (F_{ext}), for frictionless walls ($\mu^{\text{wall}}=0$) and $k_T/k_N=0.8$.

or absence of a dip in the pile geometry is determined by the degree of anisotropy in the *mechanical properties* of the pile (which is not always simply related to the anisotropy of the contact network, as shown here in the frictional case). These properties should depend on the way the pile is prepared [15].

G. Effects of applied torque

The force chains are sensitive to applied torques, whether intentional or due to the fact that (in experiments) the line of action of a force applied to a particle does not precisely pass through its center or mass. Figure 18 shows force chains in systems of 25×13 slightly polydisperse particles ($\delta=10^{-3}$) with $k_T/k_N=0.5$ and $\mu=\mu^{\text{wall}}=0.5$, for an applied force $F_{\text{ext}}=10\bar{m}g$ at 30° to the horizontal, with different applied torques. It is evident that the torques can have quite a large effect. Although their effect on the stress field (in particular, its asymmetric part) is typically confined to the vicinity of the point of application, a proper continuum description of the system requires the use of micropolar or Cosserat models [87–89].

VI. EFFECTS OF DISORDER

Ordered systems of monodisperse grains are more amenable to theoretical modeling than polydisperse systems. Real granular systems, even those nominally prepared to be monodisperse, as, e.g., in [18,22], are practically always polydisperse. Natural granular matter exhibits considerable polydispersity (also shape variability). It is therefore important to verify that the results obtained for monodisperse systems are not limited to this idealized case. We therefore performed simulations of polydisperse systems of disks, with

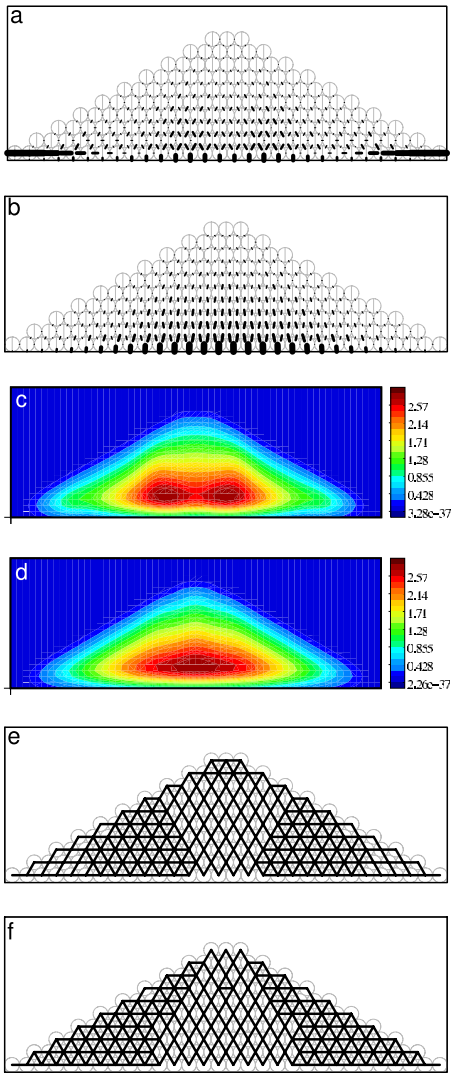

FIG. 17. (Color online) (a),(b) Interparticle forces in a pile of monodisperse disks under gravity, with (a) and without (b) friction (in the frictional case, $\mu=0.94$, $\mu^{\text{wall}}=0.35$, and $k_T/k_N=0.5$). Linewidths and lengths are proportional to the force magnitude. (c),(d) Vertical stress σ_{zz} in the same systems, calculated using a Gaussian coarse-graining function with a coarse-graining width $w=2R$. (e),(f) Contact network: contacts are depicted by lines connecting the corresponding centers of the particles.

radii distributed uniformly in the interval $[R-\delta R,R]$ (see Sec. III B), for $\delta=0.01,0.1,0.25$.

Since disorder induces force fluctuations, which are not present in ordered systems, the forces exerted on the floor were coarse grained using a Gaussian coarse-graining function in the horizontal (x) direction: $\frac{1}{w\sqrt{\pi}}e^{-(x/w)^2}$ with $w=3\bar{R}$ or $6\bar{R}$, which amounts to calculating the vertical stress σ_{zz} at the floor [90]. The stress was then averaged over several realization of the disorder (typically five).

The effect of friction on the response in disordered systems is qualitatively similar to that found in the ordered lattices described in Sec. V. Figure 19 presents a comparison of the response (averaged over 15 realizations, coarse grained with $w=3\bar{R}$) obtained in frictionless and frictional ($\mu=0.2$)

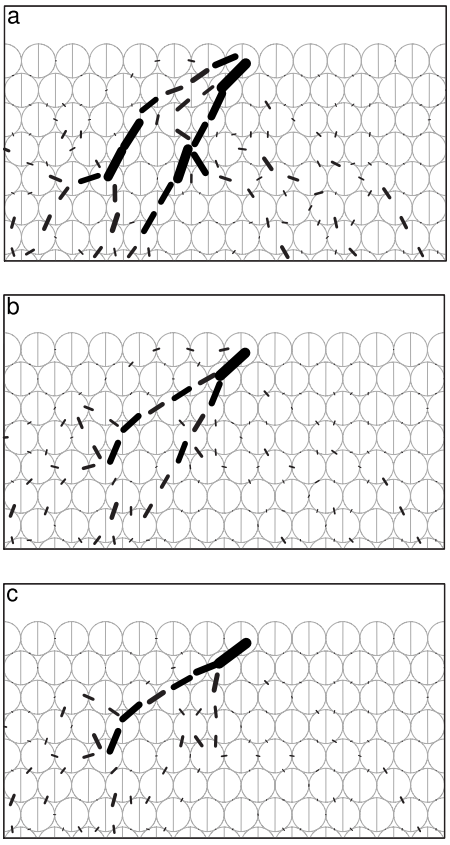

FIG. 18. Force chains in 2D packings of slightly polydisperse frictional particles ($\delta=10^{-3}$), with a force $F_{\text{ext}}=10\bar{m}g$ applied at 30° to the horizontal, and different applied torques $M=$ (a) 0, (b) $0.2F_{\text{ext}}\bar{R}$, and (c) $0.4F_{\text{ext}}\bar{R}$, in the clockwise direction. The effect of gravity has been subtracted. The same realization of the packing was used in all cases. The region shown is the central third of the upper half of the system.

disordered packings with $\delta=0.01$, and an applied force $F^{\text{ext}}=15\bar{m}g$ ($\bar{m}$ is the mean particle mass). As in the ordered case, two peaks are obtained for the frictionless systems and only one peak for the frictional ones. The fluctuations are quite large even for this small degree of polydispersity (larger for the frictionless case). For the magnitude of the force used in this case the difference between the frictionless and frictional cases is evident even for individual realizations.

A. Linearity and the crossover force

A notable difference between monodisperse and polydisperse systems is that in the latter the range of linear response is smaller than in the former (see Fig. 20 compared to Fig. 6). In order to examine the effects of polydispersity and friction we performed simulations for different degrees of polydispersity, coefficients of friction and applied forces. The results are depicted in Fig. 21. The larger the coefficient of friction, the larger the applied force at which the crossover from a single- to a double-peaked response occurs, much as in ordered systems (Sec. V A). The crossover force decreases with increasing polydispersity. Unlike the sharp transition to

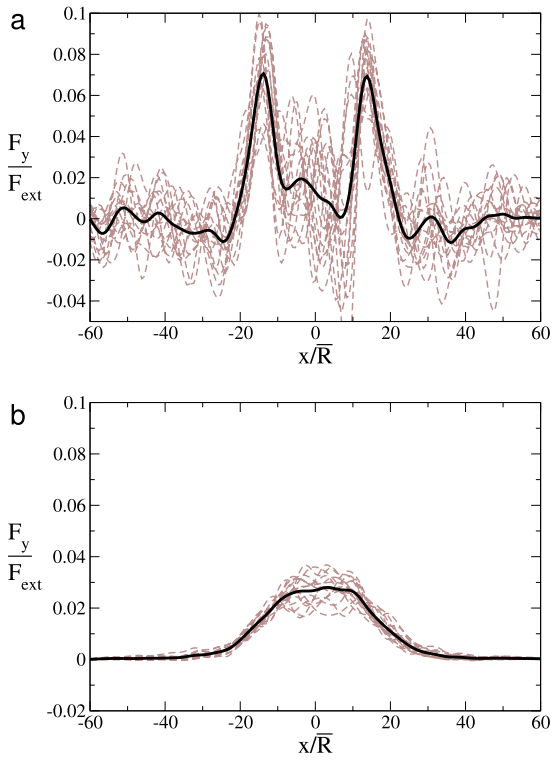

FIG. 19. (Color online) Response of (a) frictionless and (b) frictional ($\mu=\mu^{\text{wall}}=0.2$, $k_T/k_N=0.8$) disordered systems (with polydispersity $\delta=0.01$) for $F^{\text{ext}}=15\bar{m}g$ ($\bar{m}$ is the mean particle mass). Thin gray lines depict separate results for 15 individual realizations, smoothed with a Gaussian of width $w=3\bar{R}$; the thick black line corresponds to an average over these 15 configurations.

a highly asymmetric response at around $\mu=1$ in lattice configurations (Sec. V E), here the transition seems relatively smooth. A possible explanation is that, for practically any disordered realization, the response is not symmetric even for a small external force. In addition, it is basically impossible to apply very large forces to polydisperse systems without causing major rearrangements.

It is quite remarkable that an average over an ensemble of only five realizations (with coarse graining) is sufficient to obtain a clean crossover from a single peak to a double peak, and even results in nearly symmetrical profiles. It appears that, at least when the force is not too close to its crossover value, the fluctuations within the ensemble are rather small for this choice of coarse-graining length (see [90] for another set of simulations in the linear regime), so that the typical response of a realization resembles that of the ensemble average.

The results for different degrees of polydispersity can be summarized in a schematic phase diagram, Fig. 22 [1]. A more complete phase diagram would presumably depend on additional parameters which characterize the geometry of the packing (in a statistical way). A commonly used characterization of packings is that of the fabric tensors [91], often simplified by considering the distribution of contact angles. This characterization is often employed in conjunction with a mean-field approach, which fails for disordered granular materials [92,93] due to the large nonaffine component of the microscopic displacements (see also [85]).

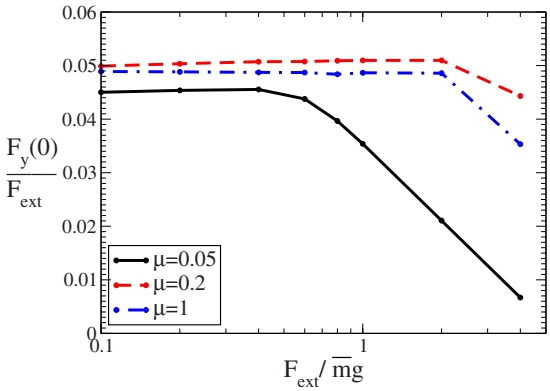

FIG. 20. (Color online) Response at $x=0$ (coarse grained with $w=3\bar{R}$) of a single polydisperse systems with $\delta=0.01$, normalized by the applied force F_{ext}, vs the applied force (in units of the mean particle weight $\bar{m}g$), for different coefficients of friction μ, with frictionless walls ($\mu^{\text{wall}}=0$), and $k_T/k_N=0.8$ (compare to Fig. 6).

Recall that in the range of polydispersity studied here the crossover force decreases with increasing disorder, i.e., polydisperse systems are more susceptible to induced anisotropy. It is possible that this result pertains to small polydispersity and a larger polydispersity may actually stabilize the system and render it more isotropic. If this is the case, the dependence of the crossover force on the degree of polydispersity should be nonmonotonic.

The nature of the crossover should also depend on the preparation method (as observed in experiments on granular piles [15] and slabs [20]). Note that in our simulations a specific preparation method was used: relaxation under gravity from a lattice configuration, so that (at least for small δ) the configuration retains partial order. Indeed, the distribution of contact angles in the systems we studied was not quite isotropic, exhibiting slightly preferred directions close to those of a triangular lattice, and therefore possessing a potential to prefer failure in specific directions.

B. Superposition

Further to the question of linearity of the response, discussed in Sec. VI A, we set out to check whether the sum of responses to several forces applied separately is the same as the response to these forces applied together. Figure 23 demonstrates a typical superposition test. Here, two downward-pointing vertical forces, each of magnitude $F_{\text{ext}}=0.2\bar{m}g$, are applied at two points (at different horizontal positions) at the top of a slab, otherwise characterized by $\delta=1\%$ and $\mu=0.05$, for which the linear range is rather small ($F_{\text{ext}} \lesssim 0.4\bar{m}g$). As shown in Fig. 23, superposition holds even on the microscopic scale, i.e., for individual forces without coarse graining; interestingly, it holds quite well even beyond the linear regime, as shown in Fig. 24 (for $F_{\text{ext}}=\bar{m}g$). A possible reason is that sufficiently far from the points of application of the forces the changes in the contact network (or sliding) are less sensitive to the precise positions of these forces. In more general terms, it is possible that the response to a distribution of forces, sufficiently far from the region

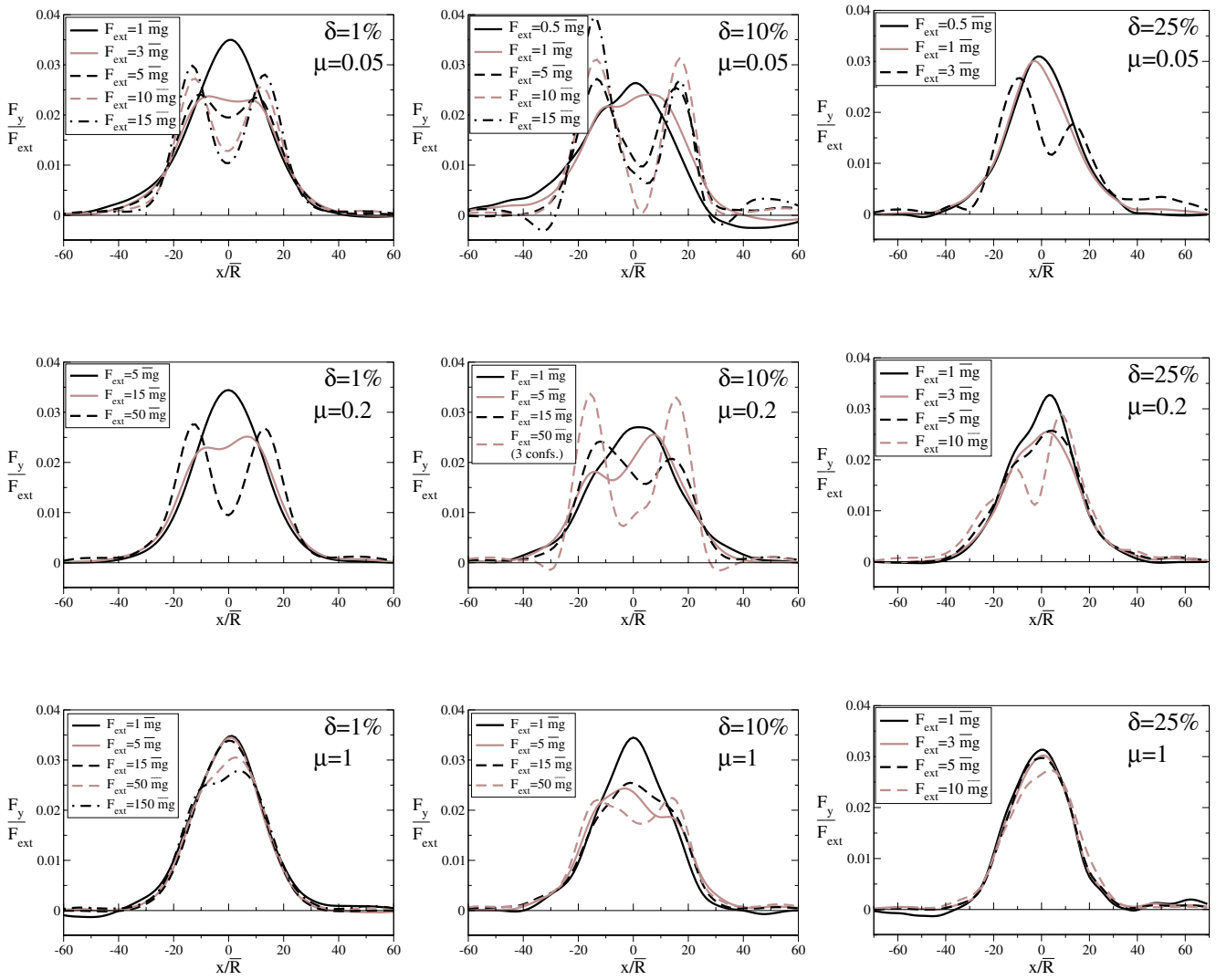

FIG. 21. (Color online) Response of disordered systems with different degrees of polydispersity δ and coefficients of friction ($\mu = \mu^{\text{wall}}$), and $k_T/k_N = 0.8$, to different applied forces F_{ext}. The response is averaged over five configurations (three for the largest force used with $\delta = 10\%$ and $\mu = 0.2$, for which the system was unstable) and smoothed with a Gaussian of width $w = 6\bar{R}$.

where they are applied, is not very sensitive to the details of the distribution. This explanation is similar to St. Venant's principle (see, e.g., [94]), which states (for a linear elastic system) that the difference in stresses and strains in the interior of an elastic body due to two separate but statically equivalent systems of surface tractions (same overall force and torque) are negligible sufficiently far from the area where the loads are applied. In the case considered here, the system is certainly not strictly elastic for $F_{\text{ext}} \gtrsim 0.4\bar{m}g$ (due to contact network changes and sliding). However, the response to a localized force (in an elastic medium) decays with the distance from the point of application as a power law [e.g., the solutions for an infinite half plane or half space (Boussinesq's problem) decay as $1/z$ in 2D and $1/z^2$ in 3D [28,52]]. Therefore, as the distance from the point of application increases, the relative displacements of the particles become smaller and elasticity becomes more appropriate a description; in particular, the response to a distributed load is the same (or nearly the same) as the response to the resultant load. This observation may apply to recent experiments [95,96] on a 2D system subject to a small cyclic displacement, which shows a $1/r$ decay of the displacement field at large distances from the perturbation.

VII. INTERPRETATION OF EXPERIMENTS

The results described in the previous section help interpret the experiments reviewed in Sec. II B. Our basic claim is that these different experiments correspond to different regions of the schematic phase diagram Fig. 22.

In the experiments on 2D systems using photoelastic particles [18,22] the applied forces were rather large; our simulations (with friction) reproduced them quite well (in these experiments the forces on the floor were not measured); see Sec. V. A full comparison with the phase diagram of Sec. VI, will require the computation of the macroscopic stress fields in these experiments.

The experiments reported in [19,20] used disordered systems and a rather small applied force (a few times the particle weight), for which a single peak was observed, in agree-

ment with the phase diagram. Since these experiments used sand, rather than spherical particles, the effective coefficient of static friction may be larger than 1, so that sliding is less likely to occur. Note that those experiments were performed on a 3D system, while the simulations reported here are in 2D; however, we expect similar qualitative features of the phase diagram for 3D systems. The difference in the response of dense and loose sand [20], as well as the deviations from the isotropic elastic prediction observed in both cases, may be explained by a small anisotropy, induced by the packing construction process (see also [97]). The anisotropy induced by the small applied force in these experiments should be negligible (note that the systems studied in [19,20] are also deeper, in terms of particle diameters, than the ones studied in [18,22]).

In contrast to the experiments reported in [19,20], those in [21], in which large forces were applied to ordered 3D packings, obtained several distinct peaks for shallow systems and diffuse peaks for deeper systems. In the absence of horizontal contacts, the coordination number in the hcp and fcc lattices is reduced to six (each particle is in contact with three particles in the layer above it and that below it). This corresponds to the (frictionless) isostatic limit. Apparently, the experimentalists attempted to avoid horizontal contacts by tuning the wall spacing; even if some horizontal contacts were initially present, it is likely that the large forces employed in these experiments opened them, at least in the top layers. The force may also have induced sliding (at least in the top layers), so that these shallow systems were extremely anisotropic, and, as mentioned, near the isostatic limit. In deeper systems there should be less opening of contacts and sliding (as we observed for $\mu=0.2$), thereby reducing the anisotropy (note that even the deepest layers in the described experiment were only about 20 layers deep). In amorphous packings, a single peak was observed (however, the method of application of the force was different: a force impulse was used, which may correspond to a weaker force in our quasistatic description). Thus, the results of the experiments reported in [21] are consistent with the schematic phase diagram presented in Sec. VI.

The phase diagram may also explain the striking difference observed in [23] between the experimentally measured displacement response in packings of (frictional) disks subject to a localized displacement (which exhibits a single peak), and the results of simulations of frictionless isostatic packings (which exhibits two peaks). Note that the mean coordination number in the frictionless polydisperse systems studied here (e.g., $z\sim 4.25$ for $\delta=0.01$) is well above the isostatic limit, $z=4$. It is, however, much smaller than that of the triangular lattice, $z=6$, the "missing" contacts being predominantly horizontal. This suggests that the hyperboliclike response of frictionless systems may arise, at least for small polydispersity, from the anisotropic structure of these systems rather than their (near) isostaticity, as suggested in [23].

VIII. CONCLUDING REMARKS

Results of simulations of the response of 2D granular slabs to an external localized force show that this force induces frictional sliding and changes in the contact network, rendering the local properties in an influence zone near its point of application *anisotropic*. When this zone spans the size of the system (as it often does in small systems), the response is anisotropic, except when frictional effects partly compensate for the loss of isotropy. It is important to notice that it is not only the contact network that determines the response but other factors as well, as detailed in this paper. In sufficiently large systems (as in most engineering applications) and/or systems subject to small applied forces, the influence zone is small compared to the system size: in this case the response is basically elasticlike and respects superposition. *Friction*, which is present in all real granular systems, increases the range of forces for which the response is linear, while further reducing the stress-induced anisotropy, often rendering the response close to that predicted by isotropic elasticity. Similar behavior is observed in (the more realistic) polydisperse systems, although they are more susceptible to the induction of anisotropy. Due to the rather small polydispersity we considered and the way we prepared the systems, the configurations were locally quasiordered. We believe that this fact should not affect our main conclusions.

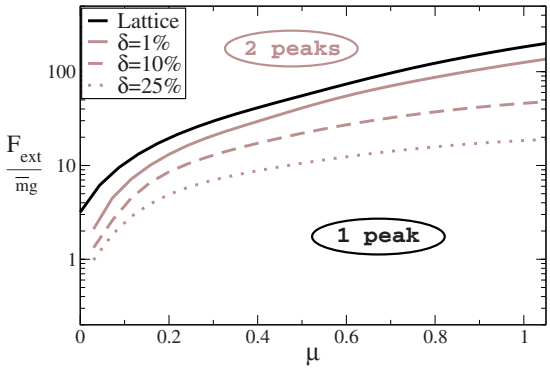

FIG. 22. (Color online) Schematic phase diagram (in the F_{ext}-μ plane) for the crossover from a single- to a double-peaked response, for different degrees of polydispersity.

The above considerations should also hold for granular piles. The properties of these piles depend on their construction history [15]: a pile grown from a point source is shaped by successive avalanches which are initiated in the apex area and is more anisotropic than one built using a nearly uniform extended source [98]. A dip in the pressure distribution at the floor was observed in the former case but not in the latter. In [15] this effect was described in terms of the orientations of force chains. We believe that the corresponding stress distributions should be compatible with anisotropic (possibly inhomogeneous) elasticity. A full elucidation of the mechanisms that are responsible for the emergence of anisotropy, in particular sliding events and contact network changes, requires further study. Anisotropy is also relevant to the distribution of stress in silos, in which the effects of wall friction and preparation are known to be of importance [99]. In our own simulations the wall friction induces nonlinear contributions to the response.

The elastic description of granular solids should be valid on sufficiently large scales (and system sizes) and for not-

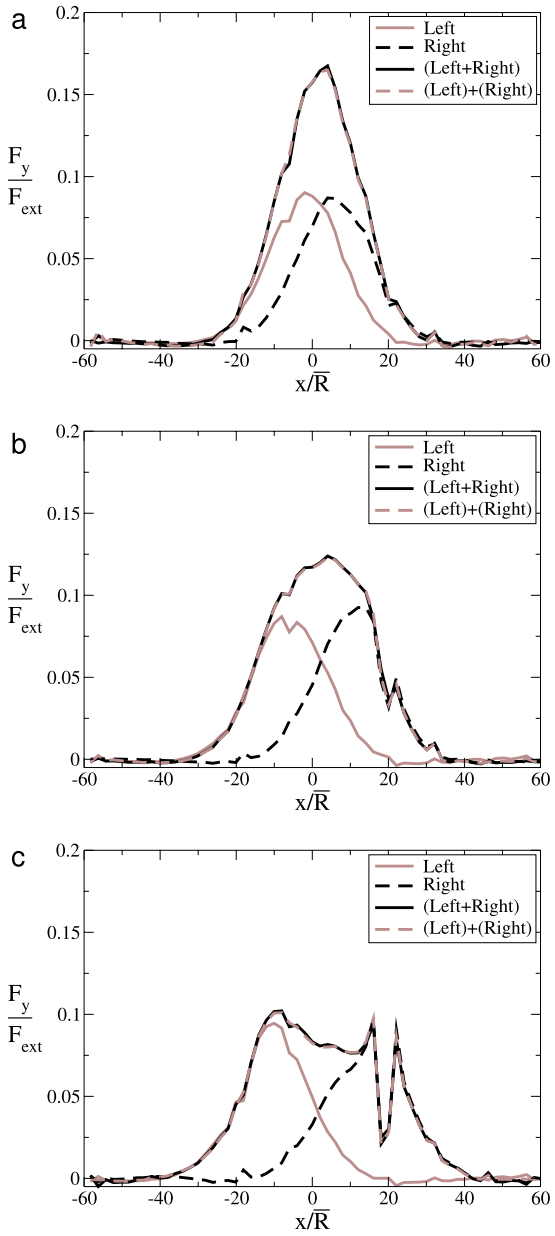

FIG. 23. (Color online) Superposition in a polydisperse system with δ=0.01, μ=0.05, F_{ext}=0.2$\bar{m}g$, frictionless walls (μ^{wall}=0), and k_T/k_N=0.8, with different distances between the points of application of the two forces (applied symmetrically with respect to the center top particle) d= (a) 8$\bar{R}$, (b) 16$\bar{R}$, and (c) 24$\bar{R}$. Lengths are given in terms of the mean particle diameter $\bar{R}$. In the legend, Left denotes the response to a force applied to the left of the center particle, Right to a force applied to its right, (Left+Right) to the two forces applied together, and (Left)+(Right) the sum of Left and Right. The shown results pertain to the forces in a single realization. Note that the dashed gray lines overlie the solid black lines (making the latter appear dashed).

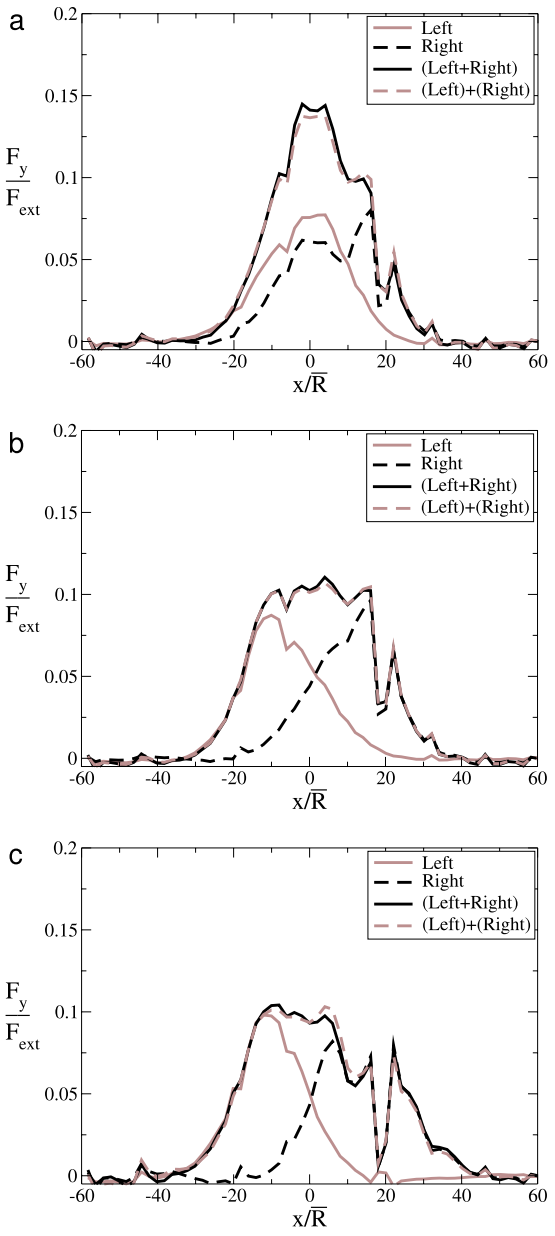

FIG. 24. (Color online) Superposition in a polydisperse system with δ=0.01, μ=0.05, and F_{ext}=$\bar{m}g$ (the same as Fig. 23 with a different applied force; the same realization of the disorder was used).

too-large applied forces. Outside this range, it needs to be amended, perhaps by using nonlinear, incrementally elastic continuum models, with stress-history-dependent elastic moduli, which represent the induced anisotropy. The nonlinear effects associated with contact breaking and frictional sliding, as well as the influence of static frictional forces, should be important for the understanding of failure (including shear banding) in granular materials. We also mentioned the possible importance of rolling resistance. All of this lends support to the suggestion that, at least on intermediate scales, continuum nonlinear models of micropolar or Cosserat type [87–89] may be required (see, e.g., [100,101]) for the modeling of granular response and beyond.

The crossover from a single- to a double-peaked response as a function of the magnitude of the applied force needs further experimental study. Systems that are sufficiently sensitive for the response to small forces (in the linear regime) to be measurable yet robust enough to withstand large exter-

nal forces are required. The forces have to be applied slowly, to avoid plastic flow.

ACKNOWLEDGMENTS

We thank A. P. F. Atman, R. P. Behringer, P. Claudin, E. Clément, J. Geng, N. Mueggenburg, M. van Hecke, W. van Saarloos, and T. A. Witten for useful discussions. We gratefully acknowledge support from the Israel Science Foundation (ISF), Grant No. 689/04, the German-Israeli Science Foundation (GIF), Grant No. 795/2003, and the U.S.-Israel Binational Science Foundation (BSF), Grant No. 2004391. C.G. acknowledges financial support from the French Ministry of Foreign Affairs and from a European Community FP6 Marie Curie Action (No. MEIF-CT2006-024970).

[1] C. Goldenberg and I. Goldhirsch, Nature (London) **435**, 188 (2005).
[2] R. M. Nedderman, *Statics and Kinematics of Granular Materials* (Cambridge University Press, Cambridge, U.K., 1992).
[3] S. B. Savage, in *Physics of Dry Granular Media*, edited by H. J. Herrmann, J. P. Hovi, and S. Luding, NATO Advanced Studies Institute, Series B: Physics (Kluwer, Dordrecht, 1998), pp. 25–95.
[4] W. Wu, E. Bauer, and D. Kolymbas, Mech. Mater. **23**, 45 (1996).
[5] G. Gudehus and K. Nubel, Geotechnique **54**, 187 (2004).
[6] J. P. Wittmer, M. E. Cates, and P. Claudin, J. Phys. I **7**, 39 (1997).
[7] A. V. Tkachenko and T. A. Witten, Phys. Rev. E **60**, 687 (1999).
[8] D. A. Head, A. V. Tkachenko, and T. A. Witten, Eur. Phys. J. E **6**, 99 (2001).
[9] S. F. Edwards and D. V. Grinev, Physica A **302**, 162 (2001).
[10] R. C. Ball and R. Blumenfeld, Phys. Rev. Lett. **88**, 115505 (2002).
[11] R. Blumenfeld, Phys. Rev. Lett. **93**, 108301 (2004).
[12] J.-P. Bouchaud, P. Claudin, M. E. Cates, and J. P. Wittmer, in *Physics of Dry Granular Media* (Ref. [3]), pp. 97–135.
[13] J. Smid and J. Novosad, Inst. Chem. Eng. Symp. Ser. **63**, D3V 1 (1981).
[14] R. Brockbank, J. M. Huntley, and R. C. Ball, J. Phys. II **7**, 1521 (1997).
[15] L. Vanel, D. Howell, D. Clark, R. P. Behringer, and E. Clément, Phys. Rev. E **60**, R5040 (1999).
[16] P. G. de Gennes, Rev. Mod. Phys. **71**, S374 (1999).
[17] M. Da Silva and J. Rajchenbach, Nature (London) **406**, 708 (2000).
[18] J. Geng, D. Howell, E. Longhi, R. P. Behringer, G. Reydellet, L. Vanel, E. Clément, and S. Luding, Phys. Rev. Lett. **87**, 035506 (2001).
[19] G. Reydellet and E. Clément, Phys. Rev. Lett. **86**, 3308 (2001).
[20] D. Serero, G. Reydellet, P. Claudin, E. Clément, and D. Levine, Eur. Phys. J. E **6**, 169 (2001).
[21] N. W. Mueggenburg, H. M. Jaeger, and S. R. Nagel, Phys. Rev. E **66**, 031304 (2002).
[22] J. Geng, G. Reydellet, E. Clément, and R. P. Behringer, Physica D **182**, 274 (2003).
[23] C. F. Moukarzel, H. Pacheco-Martínez, J. C. Ruiz-Suarez, and A. M. Vidales, Granular Matter **6**, 61 (2004).
[24] Y. Jiang and M. Liu, Eur. Phys. J. E **22**, 255 (2007).
[25] M. E. Cates, J. P. Wittmer, J.-P. Bouchaud, and P. Claudin, Chaos **9**, 511 (1999).
[26] A. Kasahara and H. Nakanishi, Phys. Rev. E **70**, 051309 (2004).
[27] S. Ostojic and D. Panja, Phys. Rev. Lett. **97**, 208001 (2006).
[28] L. Landau and E. Lifshitz, *Theory of Elasticity*, 3rd ed. (Pergamon, Oxford, 1986).
[29] C. Goldenberg and I. Goldhirsch, Phys. Rev. Lett. **89**, 084302 (2002).
[30] P. Claudin, J.-P. Bouchaud, M. E. Cates, and J. P. Wittmer, Phys. Rev. E **57**, 4441 (1998).
[31] C. F. Moukarzel, Phys. Rev. Lett. **81**, 1634 (1998).
[32] J.-N. Roux, Phys. Rev. E **61**, 6802 (2000).
[33] C. F. Moukarzel, Granular Matter **3**, 41 (2001).
[34] J.-P. Bouchaud, P. Claudin, D. Levine, and M. Otto, Eur. Phys. J. E **4**, 451 (2001).
[35] J. E. S. Socolar, D. G. Schaeffer, and P. Claudin, Eur. Phys. J. E **7**, 353 (2002).
[36] M. Otto, J.-P. Bouchaud, P. Claudin, and J. E. S. Socolar, Phys. Rev. E **67**, 031302 (2003).
[37] Y. Roichman, D. Levine, and I. Yavneh, Phys. Rev. E **70**, 061301 (2004).
[38] S. Alexander, Phys. Rep. **296**, 65 (1998).
[39] D. W. Howell and R. P. Behringer, Chaos **9**, 559 (1999).
[40] C.-H. Liu, S. R. Nagel, D. A. Schecter, S. N. Coppersmith, S. Majumdar, O. Narayan, and T. A. Witten, Science **269**, 513 (1995).
[41] S. N. Coppersmith, C.-h. Liu, S. Majumdar, O. Narayan, and T. A. Witten, Phys. Rev. E **53**, 4673 (1996).
[42] P. A. Cundall and O. D. L. Strack, Geotechnique **29**, 47 (1979).
[43] P. A. Cundall, A. Drescher, and O. D. L. Strack, in *IUTAM Conference on Deformation and Failure of Granular Materials, Delft, Holland, 1982*, edited by P. A. Vermeer and H. J. Luger (Balkema, Rotterdam, 1982), pp. 355–369.
[44] M. P. Allen and D. J. Tildesley, *Computer Simulation of Liquids* (Oxford University Press, Oxford, 1987).
[45] D. Frenkel and B. Smit, *Understanding Molecular Simulations* (Academic Press, San Diego, 1996).
[46] D. C. Rapaport, *The Art of Molecular Dynamics Simulation* (Cambridge University Press, Cambridge, U.K., 1997).
[47] R. J. Sadus, *Molecular Simulation of Fluids: Theory, Application and Object-Orientation* (Elsevier, Amsterdam, 1999).
[48] D. E. Wolf, in *Computational Physics*, edited by K. H. Hoffmann and M. Schreiber (Springer, Heidelberg, 1996), pp. 64–94.
[49] H. J. Herrmann and S. Luding, Continuum Mech. Thermodyn. **10**, 189 (1998).
[50] H. Zhu, Z. Zhou, R. Yang, and A. Yu, Chem. Eng. Sci. **62**, 3378 (2007).

[51] G. M. L. Gladwell, *Contact Problems in the Classical Theory of Elasticity* (Sijthoff & Noordhoff, Alpen aan den Rijn, The Netherlands, 1980).
[52] K. L. Johnson, *Contact Mechanics* (Cambridge University Press, Cambridge, 1985).
[53] T. Pöschel and V. Buchholtz, Phys. Rev. Lett. **71**, 3963 (1993).
[54] O. R. Walton and R. L. Braun, in Proceedings of Joint DOE/NSF Workshop on Flow of Particulates and Fluids, 1993 (unpublished).
[55] T. Pöschel and V. Buchholtz, J. Phys. I **5**, 1431 (1995).
[56] H. G. Matuttis, S. Luding, and H. J. Herrmann, Powder Technol. **109**, 278 (2000).
[57] L. Vu-Quoc, X. Zhang, and O. R. Walton, Comput. Methods Appl. Mech. Eng. **187**, 483 (2000).
[58] A. Schinner, Granular Matter **3**, 35 (2001).
[59] J. Schäfer, S. Dippel, and D. E. Wolf, J. Phys. I **6**, 5 (1996).
[60] M. H. Sadd, Q. Tai, and A. Shukla, Int. J. Non-Linear Mech. **28**, 251 (1993).
[61] O. R. Walton, in *Mobile Particulate Systems*, edited by E. Guazzelli and L. Oger (Kluwer, Dordrecht, 1995), pp. 367–380.
[62] J. Schwartz and E. Y. Harper, Int. J. Solids Struct. **7**, 1613 (1971).
[63] T. Schwager, Phys. Rev. E **75**, 051305 (2007).
[64] T. S. Majmudar, M. Sperl, S. Luding, and R. P. Behringer, Phys. Rev. Lett. **98**, 058001 (2007), supplementary information.
[65] N. V. Brilliantov, F. Spahn, J.-M. Hertzsch, and T. Pöschel, Phys. Rev. E **53**, 5382 (1996).
[66] L. Vu-Quoc and X. Zhang, Mech. Mater. **31**, 235 (1999).
[67] L. Pournin, T. M. Liebling, and A. Mocellin, Phys. Rev. E **65**, 011302 (2001).
[68] J. Krim, Am. J. Phys. **70**, 890 (2002).
[69] E. Rabinowicz, J. Appl. Phys. **22**, 1373 (1951).
[70] R. J. Bathurst and L. Rothenburg, J. Appl. Mech. **55**, 17 (1988).
[71] C. S. Chang and J. Gao, Acta Mech. **115**, 213 (1996).
[72] J. T. Jenkins and L. L. Ragione, Int. J. Solids Struct. **38**, 1063 (2001).
[73] C. Gay and R. da Silveira, Europhys. Lett. **68**, 51 (2004).
[74] L. Brendel and S. Dippel, in *Physics of Dry Granular Media* (Ref. [3]), pp. 313–318.
[75] J. Geng and R. P. Behringer (private communication).
[76] J. W. Landry and G. S. Grest, Phys. Rev. E **69**, 031303 (2004).
[77] A. P. F. Atman and P. Claudin, in *Traffic and Granular Flow 2003*, edited by S. P. Hoogendoon, S. Luding, P. H. L. Bovy, M. Schreckenberg, and D. Wolf (Springer-Verlag, Berlin, 2005), pp. 531–536.
[78] S. Luding, Phys. Rev. E **55**, 4720 (1997).
[79] M. Oda, Mech. Mater. **16**, 35 (1993).
[80] I. Goldhirsch and C. Goldenberg, in *The Physics of Granular Media*, edited by H. Hinrichsen and D. E. Wolf (Wiley-VCH, Weinheim, 2004), pp. 3–22.
[81] J. Duffy and R. D. Mindlin, J. Appl. Mech. **24**, 585 (1957).
[82] C. S. Chang and L. Ma, Int. J. Solids Struct. **29**, 1001 (1992).
[83] R. da Silveira, G. Vidalenc, and C. Gay, e-print arXiv:cond-mat/0208214.
[84] C. Goldenberg and I. Goldhirsch, Granular Matter **6**, 87 (2004).
[85] I. Goldhirsch and C. Goldenberg, Eur. Phys. J. E **9**, 245 (2002).
[86] Y. C. Zhou, B. D. Wright, R. Y. Yang, B. H. Xu, and A. Yu, Physica A **269**, 536 (1999).
[87] *Mechanics of Generalized Continua—Proceedings of the IUTAM Symposium on the Generalized Cosserat Continuum and the Continuum Theory of Dislocations with Applications*, edited by E. Kröner (Springer-Verlag, Freudenstadt, 1967).
[88] W. Jaunzemis, *Continuum Mechanics* (MacMillan, New York, 1967).
[89] A. C. Eringen, in *Fracture: An Advanced Treatise, Volume II: Mathematical Fundamentals*, edited by H. Liebowitz (Academic, New York, 1968), pp. 621–729.
[90] C. Goldenberg, A. P. F. Atman, P. Claudin, G. Combe, and I. Goldhirsch, Phys. Rev. Lett. **96**, 168001 (2006).
[91] K.-I. Kanatani, Int. J. Solids Struct. **22**, 149 (1984).
[92] C. S. Chang and C. L. Liao, Appl. Mech. Rev. **47**, 197 (1994).
[93] H. A. Makse, N. Gland, D. L. Johnson, and L. M. Schwartz, Phys. Rev. Lett. **83**, 5070 (1999).
[94] G. E. Mase, *Theory and Problems of Continuum Mechanics* (McGraw-Hill, New York, 1970).
[95] E. Kolb, J. Cviklinski, J. Lanuza, P. Claudin, and E. Clément, Phys. Rev. E **69**, 031306 (2004).
[96] E. Kolb, C. Goldenberg, S. Inagaki, and E. Clément, J. Stat. Mech.: Theory Exp. 2006 P07017.
[97] A. P. F. Atman, P. Brunet, J. Geng, G. Reydellet, G. Combe, P. Claudin, R. P. Behringer, and E. Clément, J. Phys.: Condens. Matter **17**, S2391 (2005).
[98] J. Geng, E. Longhi, R. P. Behringer, and D. W. Howell, Phys. Rev. E **64**, 060301(R) (2001).
[99] L. Vanel and E. Clément, Eur. Phys. J. B **11**, 525 (1999).
[100] R. de Borst and L. J. Sluys, Comput. Methods Appl. Mech. Eng. **90**, 805 (1991).
[101] S. D. C. Walsh and A. Tordesillas, Granular Matter **6**, 27 (2004).